Fall 2022

Advancing Understanding of the Relationship Between Tropical Cyclogenesis and Precipitation in A High-Resolution Model

Hananeh Jafary
San Jose State University

ADVANCING UNDERSTANDING OF THE RELATIONSHIP BETWEEN TROPICAL CYCLOGENESIS AND PRECIPITATION IN A HIGH-RESOLUTION MODEL

A Thesis

Presented to

The Faculty of the Department of Meteorology and Climate Science

San José State University

In Partial Fulfillment

of the Requirements for the Degree

Master of Science

by

Hananeh Jafary

December 2022

The Designated Thesis Committee Approves the Thesis Titled

ADVANCING UNDERSTANDING OF THE RELATIONSHIP BETWEEN TROPICAL CYCLOGENESIS AND PRECIPITATION IN A HIGH-RESOLUTION MODEL

by

Hananeh Jafary

APPROVED FOR THE DEPARTMENT OF METEOROLOGY AND CLIMATE SCIENCE

SAN JOSÉ STATE UNIVERSITY

December 2022

Sen Chiao, Ph.D.	Department of Interdisciplinary Studies
Ghassan J. Alaka, Jr., Ph.D.	NOAA/AOML/Hurricane Research Division
Sundararaman G. Gopalakrishnan, Ph.D.	NOAA/AOML/Hurricane Research Division
Alison F.C. Bridger, Ph.D.	Department of Meteorology and Climate Science
Qian Tan, Ph.D.	Department of Meteorology and Climate Science

ABSTRACT

ADVANCING UNDERSTANDING OF THE RELATIONSHIP BETWEEN TROPICAL CYCLOGENESIS AND PRECIPITATION IN A HIGH-RESOLUTION MODEL

by Hananeh Jafary

This study evaluates the relationship between tropical cyclone (TC) genesis, also known as tropical cyclogenesis, and precipitation in forecasts produced by the Basin-scale Hurricane Weather Research and Forecasting (HWRF-B) model. Pre-TC (PTC) forecasts from HWRF-B were produced during the 2017-2020 hurricane seasons in the North Atlantic and eastern North Pacific. In PTC forecasts, various precipitation characteristics, including rate, and coverage, were compared for different forecast outcomes of signal detection: hits, misses, false alarms, and correct rejections. Moreover, differences in radar reflectivity, mid-tropospheric moisture, and vertical wind shear (VWS) were studied and compared for developing (i.e., underwent cyclogenesis) and non-developing PTCs. In particular, we focused on comparisons between hits and false alarms (i.e., developing PTC forecasts), as well as between misses and correct negatives (i.e., non-developing PTC forecasts), to distinguish one forecast outcome from the other. In other words, the goal is to determine if developing and non-developing PTC forecasts are accurate based on precipitation, moisture, and wind shear. The result from this study indicates that the developing cases had greater maximum precipitation rates as well as a larger area coverage of higher precipitation rates at most lead/lag times. Further, VWS results revealed that non-developing disturbances also experienced weak upper-level flow. Together, these results indicate that thermodynamic properties play an important role in determining the evolution of disturbances in the North Atlantic basin.

ACKNOWLEDGEMENTS

As a graduate student, I am grateful to my advisor Dr. Chiao who welcomed me into his group and awarded me a NOAA Center for Atmospheric Sciences and Meteorology fellowship. While completing my NERTO internship, I was given the opportunity to work with experts in my field at the NOAA Atlantic Oceanographic and Meteorological Laboratory Hurricane Research Division. Throughout the entire project, my mentor Dr. Ghassan Alaka provided me with the most valuable guidance and experience. I cannot thank him enough for his endless support and encouragement. The passion he has for hurricanes has also inspired me to become a better scientist. The hurricane research division, including my co-mentor Dr. Gopalakrishnan, has been extremely helpful in listening to my presentations and providing me with outstanding feedback. The skills I gained are invaluable to my future career as a research scientist.

TABLE OF CONTENTS

LIST OF TABLES

LIST OF FIGURES

LIST OF ABBREVIATIONS

ATCF – Automated Tropical Cyclone Forecast
AEW – African Easterly Wave
AEJ – African Easterly Jet
bdeck – best track
CN – Correct Negative
CSI – Critical success index
EKE – Eddy Kinetic Energy
EMC – Environmental Modeling Center
FA – False Alarm
FAR – False Alarm Ratio
GDAS – Global Data Assimilation System
GFS – Global Forecast System
GFDL – Geophysical Fluid Dynamics Laboratory
GSI – Grid-Point Statistical Interpolation
GRIB2 – GRIdded Binary version 2
HDAS – HWRF data assimilation system
HFIP – Hurricane Forecasts Improvement Project
HMON – Hurricanes in a Multi-scale Ocean-coupled Non-hydrostatic model
Hybrid-EDMF – GFS Hybrid Eddy Diffusivity (PBL) scheme Mass-Flux
hPa – Hectopascal
HWRF – Hurricane Weather Research and Forecasting
HWRF-B – Basin-scale Hurricane Weather Research and Forecasting
ITCZ – Intertropical Convergence Zone
IMERG – Integrated Multi-satellitE Retrieval for GPM
km – kilometer
MJO – Madden-Julian oscillation
M – Meter
mb – Millibar
m/s – Meter per second
mm/h – Millimeters per hour
NOGAPS – Navy Operational Global Atmospheric Prediction System
NCEP – National Centers for Environmental Prediction
NCO – NCEP Central Operations
NHC – National Hurricane Center
NMM – Non-hydrostatic Mesoscale Model
NOAA – National Oceanic and Atmospheric Administration
NWP – Numerical Weather Prediction
NCAR – the National Center for Atmospheric Research
NOGAPS – Navy Operational Global Atmospheric Prediction System
POD – Probability of Detection
PBL – planetary boundary layer
PRTMG – Rapid Radiative Transfer Model for General circulation models

PTC – Pre-tropical cyclone
RH – Relative Humidity
SAL – Saharan air layer
SASAS –Scale-aware GFS Simplified Arakawa Schubert
SR – Success ratio
TC – Tropical Cyclone
TUTT – Tropical Upper Tropospheric Troughs
UKMET – United Kingdom METeorological
UTC – Coordinated Universal Time
VWS – Vertical Wind Shear

1. Introduction

TCs are large rotating systems that originate over warm tropical or subtropical oceans. They are enormous heat engines that draw energy from the sea surface. The water vapor contained in moist air stores this energy. As the warm moist air rises, it creates an area of low pressure. The moisture condenses and releases heat to the surroundings, causing the air to continue to rise and the neighboring air to rush in and fill the void - this is why TCs are often described as heat engines that transfer energy from the surface of tropical oceans to high in the atmosphere (Mohazzabi et al. 2022). Hurricanes have three main distinctive structures: the eye, the eyewall and rainbands on its outer edges. The hurricane eye is relatively a calm, clear area with a diameter spanning from 32-64 km (National Weather Service 2019). The strongest winds and heavy precipitation are within the dense wall of thunderstorms in the eyewall surrounding the eye. In Rogers et al. (2009), the eyewall is described as the region with the strongest updraft injecting hydrometeors into the upper troposphere. In case of intense TCs, the eyewall can extend up to 15 km with high reflectivity values and heavy convective precipitation. The curved columns of clouds and thunderstorms that lie outside of the eyewall in spiral fashion are rainbands. They include a mixture of convective and stratiform rainfall. However, the convective rainfall is much stronger in the eyewall than in the rainbands. Regions between rainbands are typically characterized by little-to-no rain and weaker winds. A convective structure in the eyewall generally is responsible for the heaviest precipitation, while, spatially outward, stratiform regions are characterized by lighter rain rates. In general, a tropical storm forms from a tropical disturbance that has organized cloud and wind patterns. However, only a small percentage of these tropical disturbances develop

into TCs (Frank and Roundy 2006). Therefore, it is a challenge for forecasters to identify in advance which disturbances will develop into a TC. Studying this weather system in its initial stages can identify gaps in understanding and eventually improve TC forecasts. Due to the potentially hazardous impacts of TCs, accurate prediction is of significant socioeconomic value. Tropical cyclones accounted for 1,083 deaths and $275.9B damages in the last 5 years alone. From the U.S. Billion-dollar disaster events, tropical cyclones dominate the chart by causing the most damage from 1980 to 2022 at $1,194.4 billion (NOAA National Centers for Environmental Information 2022)

While tropical cyclones (TCs) are officially categorized by maximum sustained surface wind speed, other parameters such as extreme rainfall, storm surge, and inland flooding play key roles in determining how much damage a hurricane is capable of inflicting. In fact, 90% of the hurricane-related deaths in the U.S between 1963 to 2012 were from water and not wind (Graham 2019). Ashraf (2019) mentions that wind speed and intense rainfall are not directly related to one another. In fact, weak storms that move slowly or stall have accounted for some of the greatest rainfall amounts (Ashraf 2019). Recent events such as Hurricane Maria (2017), Hurricane Harvey (2017) and Tropical Storm Imelda (2019) are prime examples of the destruction caused by inland flooding (Blake and Zelinsky 2018; Pasch et al. 2019; Latto and Berg 2022).

Operational forecasters use numerical models as TC guidance, including for track, intensity, and rainfall. From 2011 to 2020, track forecasts from the operational Hurricane Weather Research and Forecasting (HWRF) model improved by ~20% at all lead times. During the same time period, the HWRF intensity forecasts improved by 30-80% at 48 h and

longer lead times (Gopalakrishnan et al. 2020). While TC track and intensity forecasts have improved in the last decade mostly due to the advancement of high-resolution models, less attention has been paid to TC genesis forecasts using such models. Currently, the NHC issues the probability of TC genesis at lead times of two and five days during hurricane season (National Weather Service 2021). Nevertheless, accurate forecasting of the genesis time and location is important to predict TC intensity and track at longer lead times (Wang et al. 2018). In particular, the predictive skills of numerical models and timely forecasts of TC genesis closer to the U.S. coast may provide more accurate rainfall estimates and longer time for storm preparedness.

When a disturbance meets the criteria of a TC (i.e., closed surface circulation and organized deep convection), it is determined to have undergone tropical cyclogenesis or TC genesis. Although the definition of TC genesis is straightforward, it often depends on a delicate balance of environmental factors. Over the last several decades, many studies identified environmental factors that influence TC genesis using satellite, numerical weather prediction models, and field campaigns (Palmén 1948; Gray 1968, 1977, 1998; McBride and Zehr 1981; Wang 2012; McTaggart-Cowan et al. 2013; Galarneau et al. 2015; Bentley et al. 2017). In the North Atlantic, the majority of TC genesis events occur within an environment characterized by: 1) a deep marine mixed layer with sea surface temperature of at least 26.5°C (Palmén 1948; Gray 1968); 2) A pre-existing low-level disturbance (Gray 1968); 3) high mid-troposphere moisture situated in an area of organized deep convection with large-scale ascending motion (Gray 1968); and 4) weak-to-moderate vertical wind shear (VWS; Gray 1968; McBride and Zehr 1981). Palmén (1948) discovered that TCs typically form

away from the equator where the sea surface temperature (SST) is greater than 26 °C. McBride and Zehr (1981) concluded that TC genesis benefits from weak or no easterly VWS. Gray's (1968) TC genesis climatology work summarized several environmental conditions that are crucial in causing TC genesis in the current climate.

Despite decades of research, a complete understanding of TC genesis formation remains ambiguous. This is indicated by the number of proposed TC genesis theories and their discrepancies. Previous literature has usually presented the development of TC formation as following either a "top-down" or "bottom-up" pathway. In the top-down theory, a TC generally develops when a mid-tropospheric mesoscale cyclonic vortex forms in a stratiform rain region and, subsequently, initiates a surface cyclonic circulation beneath it. In the bottom-up pathway, genesis evolves from the axis symmetrization of multiple small-intense vortical convective towers preconditioning the lower troposphere (Hendricks et al. 2004; Montgomery et al. 2006). However, previous studies suggest that genesis can emerge from the contribution of multiple precipitation modes instead of a few deep convective clouds (Wang 2012; Fritz et al. 2016). The conditions favorable for achieving TC genesis can be satisfied by a range of precursor disturbances such as an African easterly wave (AEW), which contributes to the formation of 70% of Atlantic tropical cyclones. Tropical upper tropospheric troughs (TUTT) can provide effective environments for TC genesis, as well.

Wang (2012) studied thermodynamic aspects of two areas near the circulation for developing TC. Wang summarized that while convective precipitation plays an important role in spinning up the low-level circulation, the stratiform heating induces moderate midlevel inflows and very weak low-level outflows. This suggests that stratiform heating

contributes to the midlevel spin-up without substantially affecting the low-level circulation. Fritz et al. (2016) further examined different types of precipitation and their key roles in TC formation and suggested that the fate of TC formation depends on the contribution of all types of precipitation rather than one. The contribution from stratiform precipitation was consistent with the previous study. The upper tropospheric heating is associated with high frequency of occurrence of stratiform precipitation and its broad areal coverage. This can influence the storm intensity and the warm-core structure. Previous studies theorize that disturbance's thermodynamic and kinematic structure is likely to be closely tied to precipitation processes (Zawislak 2020; Rogers et al. 2020). Suppose large-scale conditions are favorable for TC generation. In that case, the evolutionary fate of the TC may depend on how kinematic and thermodynamic structures of the inner core respond to the precipitation organization within the disturbance Zawislak (2020). This multiscale interaction is also consistent with the framework described by Rogers et al. (2020). The study concluded that changes in the thermodynamic environment drove changes in the precipitation structure, while precipitation impacted the local environment in a way that influenced future rainfall occurrences. Moisture in the upper troposphere is increased by deep convection, while shallow and moderate convection can moisten low- to mid-level troposphere. Therefore, convection can modify the thermodynamic profile in a pre-TC, leading to deeper and more persistent convection. The uptick in convection induces strong low-level convergence that is capable of spinning up a low-level circulation.

It is not a new idea that large-scale, equatorial waves can enhance or suppress tropical cyclogenesis. One of the earlier studies that analyzed the structures of these waves was done

by Matsuno (1966). The study summarized various types of equatorial waves that generally move zonally along the equator: Kelvin waves, Rossby waves, and inertio-gravity waves. These waves exist in different parts of wavenumber-frequency space, with inertio-gravity (Rossby) waves having the highest (lowest) frequency. Rossby waves propagate westward, Kelvin waves propagate eastward, and inertio-gravity waves can propagate in either direction.

Later, the Madden-Julian oscillation (MJO) was discovered as an additional equatorial wave that propagates slowly eastward at large wavenumbers (Madden and Julian 1971, 1972, 1994; Wheeler and Kiladis 1999). Hartmann and Maloney (2001) examined that the opposite of the strong 850-mb anomalous westerlies and easterlies over the tropical eastern and western North Pacific Ocean represents a phase of Madden-Julian oscillation (MJO) during summer in the northern hemisphere. The barotropic conversion from the mean low-level flow generates eddy kinetic energy (EKE) when 850-mb wind anomalies associated with the MJO are westerly. The eddies can then seed tropical disturbances. Frank and Roundy (2006) has shown that different types of equatorial waves play significant roles in causing (or denying) TC genesis. These equatorial waves have been shown to modulate the synoptic scale environment, e.g., anomalous ascent (descent) to encourage (discourage) TC genesis (Frank and Roundy 2006; Ventrice et al. 2011, 2012). Alaka and Maloney (2012), identified how MJO influences large scale environments in tropical North Africa. During the wet phase, MJO may enhance convection and the African easterly jet (AEJ), ultimately producing a period of stronger AEW activity. Similarly, less convection during the dry MJO phase may

reduce AEW activity. The next paragraph will discuss the importance of AEW in TC formation.

TCs in the North Atlantic most commonly develop from AEWs, which are one of the main synoptic-scale features in tropical North Africa. These waves form on the AEJ in boreal summer through a mixed baroclinic-barotropic growth mechanism and propagate westward across Africa and the North Atlantic and, sometimes, into the eastern North Pacific. They have wavelengths that range from 2000-4000 km, phase speeds that range from 7-9 m/s and peak amplitudes at around 600-700 hPa (close to the level of the AEJ). Approximately 50–60 waves develop each year over North Africa, and the majority of them propagate into the North Atlantic Ocean (Avila et al. 2000; Avila and Pasch 1992). Enyew and Mekonnen (2022) found that an average of ~20% of the AEWs that cross the West African coast develop into TCs, although there is significant year-to-year variability. Therefore, it is important to understand the influence of AEWs on TC genesis. Seo et al. (2008) found that there is a close correlation between strong cyclonic wind shear introduced by an AEW's horizontal winds and strong precipitation as indicated by increased localized precipitation that is observed with large amplitudes of these waves. Regions of high cyclonic shear in easterly waves experience heavy precipitation events which correlate to significantly enhanced near-surface convergence. As a result of the cyclonic shear associated with waves, stronger convergence occurs near the surface, which triggers convection and, in turn, produces more intense precipitation. As AEWs propagate westward, a favorable (unfavorable) large-scale environment, including VWS, mid-to-upper tropospheric moisture, and sea surface temperature can enhance (reduce) the development of these waves. Agudelo

et al. (2011) suggested that occurrence of TC genesis increases when the AEW is accompanied by moist convection and pre-existing large-scale convergence. According to Enyew and Mekonnen (2022), AEWs that developed into TCs showed higher relative humidity (RH) over a large area around the AEW axis and to the west as well as strong circulation. Non-developing AEWs showed negative relative humidity anomalies in the middle and upper troposphere that limits wave growth. Peng et al. (2012) also pointed out that a dry signal can also be seen just ahead of the AEW trough at mid-to-upper levels in the non-developing AEW. From these studies, it is evident that AEWs play a critical role in TC formation.

Although there has been a significant improvement in forecasting the early stages of TC, there is still much uncertainty in predicting these events. Improving TC genesis forecasts requires understanding the state of the large-scale environment adjacent to pre-TCs and the distribution and type of precipitation within these disturbances. An improvement in our understanding of TC formation may develop through an evaluation of precipitation in high-resolution hurricane models. Despite the substantial improvement in the hurricane track forecast, prediction of TC genesis remains a challenge for both regional and global models. This is because a TC track is controlled by environmental flow and synoptic-scale interactions, which are reasonably predictable (Elsberry et al. 2013; Davis et al. 2008). In contrast, TC genesis is influenced by multi-scale processes. Since TCs form over the open ocean where in situ observations are rare, we heavily rely on models to resolve critical features that lead to TC genesis. Numerical weather prediction (NWP) models have improved significantly over the last decade. In the United States, during hurricane season, the

National Hurricane Center (NHC), one of the National Centers for Environmental Prediction (NCEP) in the National Weather Service (NWS) of the U. S. National Oceanic and Atmospheric Administration (NOAA), utilizes global and high-resolution regional models to provide guidance and conduct research about TC track and intensity. In 2017, the two operational high-resolution regional NWP models known as the Hurricanes in a Multi-scale Ocean-coupled Non-hydrostatic model (HMON) and the HWRF underwent a significant upgrade (Mehra et al. 2018). There were several HWRF model infrastructure advancements such as increased vertical resolution from 61 to 75 levels, upgrades to physics parameterizations (e.g., cumulus scheme), and implementation of the newest version of Geophysical Fluid Dynamics Laboratory (GFDL) vortex tracker. Refer to the Mehra et al. (2018) for more details about 2017 upgrades. The very high resolutions of the innermost nested domains of HWRF (4.5 km and 1.5 km, respectively) can resolve TC inner core structures such as eyewall, eyewall replacement, and spiral rainbands (Dong et al. 2020; Alaka et al. 2022). These improvements in high-resolution models have greatly improved our understanding of TC formation. However, it is not yet possible to rely entirely on weather models to resolve complex, multiscale processes that occur with the evolution of TC genesis. For instance, microphysical processes, planetary boundary layer (PBL) processes, and convection are all parameterized (Halperin et al. 2013). In addition, computational limitations and grid spacing restrain models from fully resolving all atmospheric processes necessary for TC genesis. Despite the caveats above, hurricane models generally produce TC-like evolution in the forecast fields.

Early studies in the North Atlantic also investigated the skill of various models in accurately predicting TC genesis. Beven (1999) concluded that although some models accurately predicted TC genesis, they often generated spurious TCs, i.e., they did not develop in reality. That indicates a propensity for a high hit rate as well as a high false alarm rate. In contrast, a TC may develop in reality that the models did not predict (i.e., a miss). During the 2005 North Atlantic season, the prediction of TC genesis was compared in NOAA's Global Forecast System (GFS), the Navy Operational Global Atmospheric Prediction System (NOGAPS), and the Met Office global model (UKMET) models. Based on the results, GFS had the highest number of false alarms (FAs), but also the highest probability of detection (POD) as well. By contrast, NOGAPS had the lowest POD and FA ratio. The accuracy of TC genesis forecasts differs significantly from one TC to another, according to Pasch et al. (2008). As Halperin et al. (2013) mentioned, GFS accurately predicted the genesis of Dean (a category five hurricane) many days in advance. Still, it failed to forecast Felix (another category five hurricane) just several weeks later.

Our focus is to analyze precipitation characteristics and identify distinguished properties associated with developing and non-developing tropical disturbances. It is also crucial to determine if the high-resolution Basin-scale Hurricane Weather Research and Forecasting (HWRF-B) system can accurately forecast the fate of pre-genesis disturbances in the North Atlantic basin. There has been a considerable effort and investment in improving TC track and intensity forecasts derived from models. In contrast, very few studies have examined if models can predict TC genesis in the North Atlantic basin. This study will utilize a high-resolution hurricane model to investigate two main points: 1) the relationship between

precipitation and TC genesis and 2) the effect of the local environment on precipitation in all developing and non-developing cases. A large data set, categorized into developing (pregenesis stage) and non-developing disturbances (described more in section 2), is used to facilitate composite analyses over multiple years of cases in the North Atlantic basin.

This paper has four sections: section 2 covers the background and methodologies employed to evaluate the composite forecasts. The results are presented in section 3, and section 4 provides concluding remarks.

2. Methodology

2.1 HWRF Model

The HWRF model has been critical to advancing NWP of TCs for over a decade. In 2007, the HWRF model was developed at NOAA's NWS/Environmental Modeling Center (EMC) and became operational at NCEP to advance our basic understanding of TCs and accelerate TC forecast improvements (Gopalakrishnan et al. 2011, 2012, 2013; Atlas et al. 2015; Bao et al. 2012; Tallapragada et al. 2014; Mehra et al. 2018). Annual changes to the HWRF system are made based on retrospective testing and upgrades to the Global Data Assimilation System (GDAS) and GFS, which provides initial and lateral boundary conditions for HWRF. Annual upgrades are approved by the NHC prior to the start of the eastern North Pacific and North Atlantic hurricane seasons (15 May and 1 June, respectively) and implemented by the NCEP Central Operations (NCO). This allows NHC forecasters to utilize the improved hurricane guidance at the start of each hurricane season (Biswas et al. 2018a).

To address the increasing vulnerability of the United States to the disastrous consequences of tropical cyclones (TC), the Hurricane Forecasts Improvement Project (HFIP) was created in 2008. It is a collaborative effort between government agencies and academic institutions in the United States to improve TC forecast guidance and our understanding of TC dynamics. The HWRF model is one of the dynamical models being upgraded as part of HFIP (Gall et al. 2013; Gopalakrishnan et al. 2020). In response to the HFIP's goal, the HWRF system received several enhancements. The upgrades to the model physics have been transferred to the operational HWRF model that led to the improvement of

intensity and forecast skills. The transition and evaluation of the updated PBL scheme is documented in W. Zhang et al. (2015). HWRF data assimilation system (HDAS) improvements included three techniques for hybrid ensemble-variational data assimilation. The Grid-Point Statistical Interpolation (GSI)-based HDAS can provide the initial size, intensity, structure, and location of the inner core of a TC (Mehra et al. 2018).

Prior to 2012, HWRF had only one moving nest per storm. There are now two telescoping moving nests per storm. With the support of NOAA's HFIP, the new TC forecasts system was transitioned into operations in 2012 (X. Zhang et al. 2016). The V4.0a is the latest community version of the operational HWRF model configured with three domains. The latest version includes an upgrade in the horizontal resolution. The new parent domain is 13.5-km and 4.5/1.5 km for the two nested domains, while the previous resolution was set to 18/6/2 km for each domain respectively (Biswas et al. 2018a, 2018b). The high-resolution moving nests have several key advantages, including: 1) resolving TC inner core structures, 2) the intensity forecast is improved as more advanced physics packages and data assimilations are integrated into the model, 3) computationally efficient since these nests are confined to a small area around the TC (Alaka et al. 2022). Refer to Table 1 for more details about HWRF's configuration options.

2.2 HWRF-B Model

As mentioned in the previous paragraph, the operational HWRF model is storm-centric, meaning there are two high-resolution, telescopic nests following one storm per forecast integration. This is not ideal for studying storm-environment interaction, storm-storm interactions, or TC genesis. In addition, the HWRF model outermost domain has limited size,

Configuration options	HWRF-B	Operational HWRF (v4.0a)
Parent Domain	**194° x 84.2°** @ 13.5 km	**77.2° x 77.2°** @ 13.5 km
Outer Moving Nest	**16.5° × 16.5°** @ 4.5 km	**17.8° × 17.8°** @ 4.5 km
Inner Moving Nest	**5.5° × 5.5°** @ 1.5 km	**5.9° × 5.9°** @ 1.5 km
Multi-Storm	**Yes, moving nests for up to 5 TCs**	**No, moving nests for only 1 TC**
Vertical Levels	75 hybrid pressure-sigma	Same as HWRF-B
Model top	10hPa	Same as HWRF-B
Microphysics scheme	Ferrier- Aligo	Same as HWRF-B
Radiation scheme	Rapid Radiative Transfer Model for General circulation models (PRTMG)	Same as HWRF-B
Cumulus scheme	Scale-aware GFS Simplified Arakawa Schubert (SASAS)	Same as HWRF-B
Planetary Boundary Layer	GFS Hybrid Eddy Diffusivity (PBL) scheme Mass-Flux (Hybrid-EDMF)	Same as HWRF-B
Shallow cumulus convection	Mass-Flux approach	Same as HWRF-B

Table 1. List of configuration options for HWRF-B and operational HWRF (v4.0a), with differences in boldface.

which prevents the enhancement of forecast skills beyond five days. For this reason, with the support of HFIP, the HWRF-B was developed with two advanced configuration options: 1) a large, fixed outermost domain that covers the eastern North Pacific and entire North Atlantic hurricane basins, and 2) multiple high resolution moving telescopic nests each following tropical systems (Gopalakrishnan et al. 2020; Biswas et al. 2018b). In this study, the 2020 version of HWRF-B is used to understand the relationship between TC and precipitation. The following information about the HWRF-B configuration options, including physics parameterization schemes, are stated in Alaka et al. (2020). HWRF-B model is a research NWP model that uses the Non-hydrostatic Mesoscale Model (NMM) dynamical core identical to the HWRF model. In 2018, HWRF-B updated the model resolution to 13.5/4.5/1.5 km for each domain, respectively. A study from Roberts and Lean (2008) stated that finer resolution can improve predictions of heavier precipitation and localized rain, making the HWRF-B model ideal to study precipitation. Both models are regional and

identical in atmospheric configuration. Table 1. represents the key configuration options for HWRF-B and HWRF models.

2.3 Invest Forecast Files and Data

We evaluated 415 potential TC, i.e., "invest", forecasts made by HWRF-B in the North Atlantic basin from 2017-2020. Typically, a disturbance is classified as an invest (area of investigation) if it has the potential to become a TC. NHC officially defines an invest as a weather system for which a TC forecast center (e.g., NHC, Central Pacific Hurricane Center, Joint Typhoon Warning Center) is interested in collecting specialized data sets (e.g., microwave imagery) and/or running model guidance (NOAA National Hurricane Center n.d.). For the data analyzed in this study, HWRF-B only initiated high-resolution moving nests for disturbances classified as invests or TCs. In other words, moving nests were not provided to disturbances that had a near-zero probability of development.

The HWRF-B model produces several types of forecast products, such as total precipitation, instantaneous precipitation rate, tracker output with the location and maximum sustained wind, and several three-dimensional atmospheric fields. Most products (e.g., precipitation rate, RH, VWS, tracker) are available every 3 h from 0-126 h, while the total precipitation total is available every 1 h over the same forecast period. Precipitation rate is evaluated from the innermost moving nest with grid spacing of 0.015°. RH and VWS are evaluated from the parent domain with 0.25° resolution. The total precipitation is produced as a swath from the innermost moving nest with 0.05° resolution. The precipitation swath is accumulated at each lat/lon grid point as the moving nest passes over. The TC centers are identified using the GFDL vortex tracker in Automated Tropical Cyclone Forecast (ATCF)

format. This tracker software examines model forecast output to provide a best guess of the storm center location, in addition to other metrics such as maximum sustained wind, mean sea level pressure, and the radius of gale-, storm-, and hurricane-force winds (Biswas et al. 2018c). Note that the tracker output is not available after the storm dissipates if that occurs before the end of the forecast period (126 h). The GFDL tracker is not used to track the storm center (and, subsequently, move the nest) within the HWRF-B model integration because it is too expensive to run at every time step. Therefore, HWRF-B uses a simplified, internal tracker to estimate the center of the storm and, concurrently, to move the nest to that location at every time step. This can create discrepancies between the GFDL and internal trackers that are larger for weaker disturbances. As a result, these invest forecasts were excluded from the final composites because part or all of the storm was outside the innermost moving nest domain. The HWRF-B forecasts are verified with the post-processed best track (bdeck) data. In order to improve operational efficiency, NHC uses the ATCF system. This software provides TC "fix" observations as well as updates to the "working" bdeck (Rappaport et al. 2009). The NHC provides this data in ATCF format, consistent with the GFDL tracker format.

2.4 Definition of TC Genesis

The NHC defines TC genesis as follows: synoptic-scale non-frontal cyclone with a warm core, persistent and organized deep convection, and a closed near surface circulation around a well-defined center (NOAA National Hurricane Center n.d.). The genesis should also meet the minimum sustained surface wind speed threshold of 17 m/s (34 knots). It is difficult to come up with a single definition of genesis that fits all needs, even though there are

operationally driven definitions of genesis, such as the first appearance of a tropical depression or storm based in bdeck records. It is therefore vital, from a research viewpoint, to recognize that genesis is a continuous, complex, and multiscale process that occurs over time. In fact, topics that are related to this study have defined model-indicated genesis differently (e.g., Tang et al. 2020; Halperin et al. 2013). Two studies done by Marchok (2002) and Walsh et al. (2007) showed that depending on the model resolution, parameters that define genesis have different thresholds. The definition of genesis in this study is as follows:

1. A PTC was determined to have developed into a TC (i.e., has undergone tropical cyclogenesis) when the maximum sustained 10-m wind speed is equal or above 34 knots for at least 12 consecutive hours.
2. A non-developing PTC is defined as when the system fails to meet the minimum conditions. For example, a PTC that only briefly reached a maximum wind speed intensity of ≥ 34 kt was not considered to have robustly exhibited cyclogenesis and may not even have a closed low-level circulation, a requirement of tropical cyclogenesis or when the maximum speed corresponds to convective activity that generally occurs in shorter time scale.

It should be noted that this genesis definition does not explicitly require a closed surface circulation for a system to be considered a TC, which is a genesis requirement in the NHC definition. Therefore, real TCs and model TCs have slightly different definitions, and this difference is a caveat of the study. However, removing the closed circulation criteria allowed a determination of genesis entirely from the ATCF data and provided a larger sample of developing disturbances.

2.5 Classification of Developing and Non-Developing Cases

A contingency table was constructed to evaluate the performance of HWRF-B cyclogenesis forecasts. All the non-developing developing PTCs were then classified into four categories based on the following criteria:

Hit (H) — TC genesis is forecasted in both HWRF-B and bdeck.

False Alarm (FA) — TC genesis is forecasted in HWRF-B, but not in bdeck.

Correct Negative (CN) — TC genesis is not forecasted in both HWRF-B and bdeck.

Miss (M) — TC genesis is not forecasted in HWRF-B, but it occurs in bdeck.

For simplicity, a "critical time" is defined as the genesis time in all the developing cases and time of maximum intensity in the Misses and CN categories. In the Hit and FA categories (i.e., developing cases), the critical time is defined as the first lead time that the storm had maximum sustained surface winds of at least 34 knots. Since some of the non-developing PTCs never reached 34 knots; therefore, the critical time is the first hour that the maximum wind speed is reached in those invest forecast files.

In order to determine the differences between the developing and non-developing groups and to understand the dynamic and thermodynamic processes that underlie these differences, lead/lag composites of key analysis fields are evaluated over a 5-day period (day -2, -1, 0, 1, 2) centered on the critical time. Storm-scale composites are computed within a storm-centered 3° x 3° box from moving nest output (0.015°), and large-scale composites are computed within a storm-centered 10° x 10° region from the parent grid output (0.25°). The composite at the critical time (e.g., day 0) has the largest number of cases, and case numbers decrease as lead/lag time increases. The discrepancy in case numbers occurs in forecasts

when the critical time is close to the initial lead time (0 h) or the final lead time (126 h), meaning lead or lag times are actually outside of the forecast period in these cases and, therefore, are unavailable. As a result, the number of cases was homogenized across each five-day analysis period, i.e., the forecast must be available at every analysis time to be included in the composite. There are pros and cons to this method. While there will be fewer sample cases to examine, the forecasts included in the composites for a given event type will be identical. Furthermore, Table 2 represents some of the storms that had to be removed due to missing GRIdded Binary version 2 (GRIB2) files and/or if we observed an unusual precipitation pattern. Technical difficulties limited the application of this technique only to the days prior to the critical time. Finally, if there is a discrepancy between simplified and GFDL tracker storm centers, sometime can occur at the edge of the plot. Sometimes, discrepancies between simplified and GFDL tracker storm centers can occur at the edges of the plot - these cases are removed from the composite. In addition to evaluating the precipitation rate plots, the following method is used. Ko et al. (2020) evaluated precipitation rates from the HWRF-B model for Hurricane Harvey in 2017. The study classified light precipitation as (< 5 mm h^{-1}), moderate as (6-10 mm h^{-1}), and heavy as (> 10 mm h^{-1}). This study also used the same classification to identify precipitation rate.

Forecast Initialization Time	Storms' Names
1200 UTC 20 September 2019	Karen (AL122019)
1200 UTC 21 September 2019	Karen (AL092019)
0600 UTC 18 October 2020	Epsilon (AL272020)
1800 UTC 01 October 2020	Gamma (AL252020)
1800 UTC 08 November 2020	Theta (AL302020)

Table 2. Removed cases from the composite with an unusual precipitation pattern.

It is important to employ statistical analysis to determine the model performance. In this study, we analyzed HWRF-B skill by calculating traditional metrics from the contingency table. Some of these verification methods are critical success index (CSI; equation 1), probability of detection (POD; equation 2), success ratio (SR; equation 3), false alarm ratio (FAR; equation 4), and bias (equation 5).

$$\textbf{Critical Success Index} = \frac{H}{H+FA+M} \quad (1) \qquad \textbf{Probability of Detection} = \frac{H}{H+M} \quad (2)$$

$$\textbf{Success Ratio} = \frac{H}{H+FA} \quad (3) \qquad \textbf{False Alarm Ratio} = \frac{FA}{H+FA} \quad (4)$$

$$\textbf{Bias} = \frac{H+FA}{H+M} \quad (5)$$

H = Hits **M** = Misses

FA = False Alarms **CN** = Correct Negatives

All the statistical measurements above are plotted on a performance diagram (Figure 1). It is a method that is conceptually comparable to the Taylor (2001) diagram. It is a good way of visually understanding the relationship between the four elements of the contingency table. A perfect forecast requires CSI, SR, POD, and bias score to approach unity.

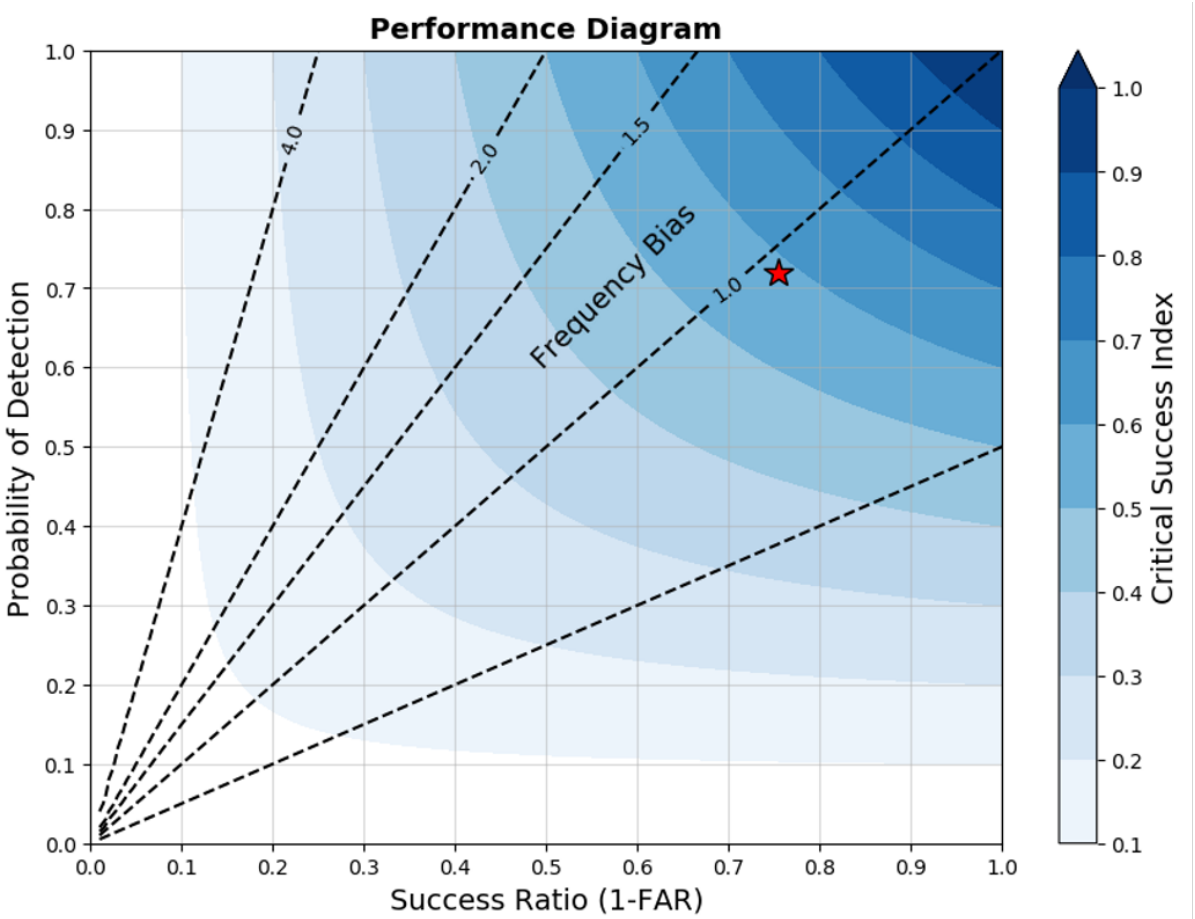

Figure 1. Performance diagram for TC genesis forecasts made by the HWRF-B model. The x-axis is the success ratio (SR), and the y-axis is the probability of detection (POD). Dashed lines indicate frequency bias increasing counter-clockwise. Blue shading indicates the critical success index (CSI) increasing toward the upper right. Perfect forecasts will be at the top right corner, and forecasts that are always wrong will be at the bottom left corner.

3. Results

3.1 Outcome of the Contingency Table and Performance Metrics

The result of the statistical analysis from our contingency table is displayed in Figure 2. From 2017 to 2020, the total number of invest forecasts was 415, including 169 hits, 125 correct negatives, 55 false alarms, and 66 misses. Following the calculation, HWRF-B SR is 75.4%, CSI is 58.3%, POD is 71.9%, and FA rate is 24.6%. Our genesis definition is used to calculate these values. Therefore, we can have different values if we restrict or simplify the genesis definition.

Total Cases: N = 415		*HWRF-B Genesis?*	
		Yes	*No*
Observed Genesis?	*Yes*	**H = 169**	**M = 66**
	No	**FA = 55**	**CN = 125**

Figure 2. A traditional contingency table is constructed to evaluate HWRF-B performance for TC genesis. HWRF-B invest forecasts are compared with NHC observations in the North Atlantic from 2017-2020.

3.2 Developing Cases (Hits and False Alarms)

3.2.1 PRECIPITATION RATE

This section evaluates precipitation rate for Hit and FA events. The mean precipitation rate evolution leading up to TC genesis for hits and FAs is shown in Figure 3. For hits, precipitation rates are mostly light (< 2 mm h^{-1}) at -48 h and -24 h, with a few isolated maxima that meet moderate and heavy classifications (Figure 3a,b). By 0 h (i.e., the critical time), precipitation rates increase dramatically near the storm center, with moderate precipitation rates extending at least 1° away from the center and isolated very heavy rainfall rates greater than 15 mm h^{-1} embedded within (Figure 3c). Furthermore, the area of rainfall rates greater than 1 mm h^{-1} increases from -24 h to 0 h. The precipitation rate composites are suggestive of curved bands at the critical time, especially to the west and north of the storm center. In fact, the band to the west of the center had a large area of rainfall rates > 4 mm h^{-1}.

The precipitation rate evolution for FAs is somewhat similar to the hit category because it gradually increases approaching the critical time (Figure 3d-f). However, the precipitation rates were much lower prior to genesis, with a larger area producing rain rates < 0.5 mm h^{-1} than for hits. Precipitation rates increased intensely in the 24-h period before genesis, including the area coverage of moderate and heavy precipitation rates. Despite the overall increase in precipitation rate, the area of > 1 mm h^{-1} rates was much smaller than for hits. Another key difference at the critical time is weaker precipitation rates in all the quadrants for FAs compared to the hits.

Figure 4 illustrates the positive hours for hit and FA. Only the main points will be discussed in order to reduce redundancy. In the hits category, the mean rain rates appeared to

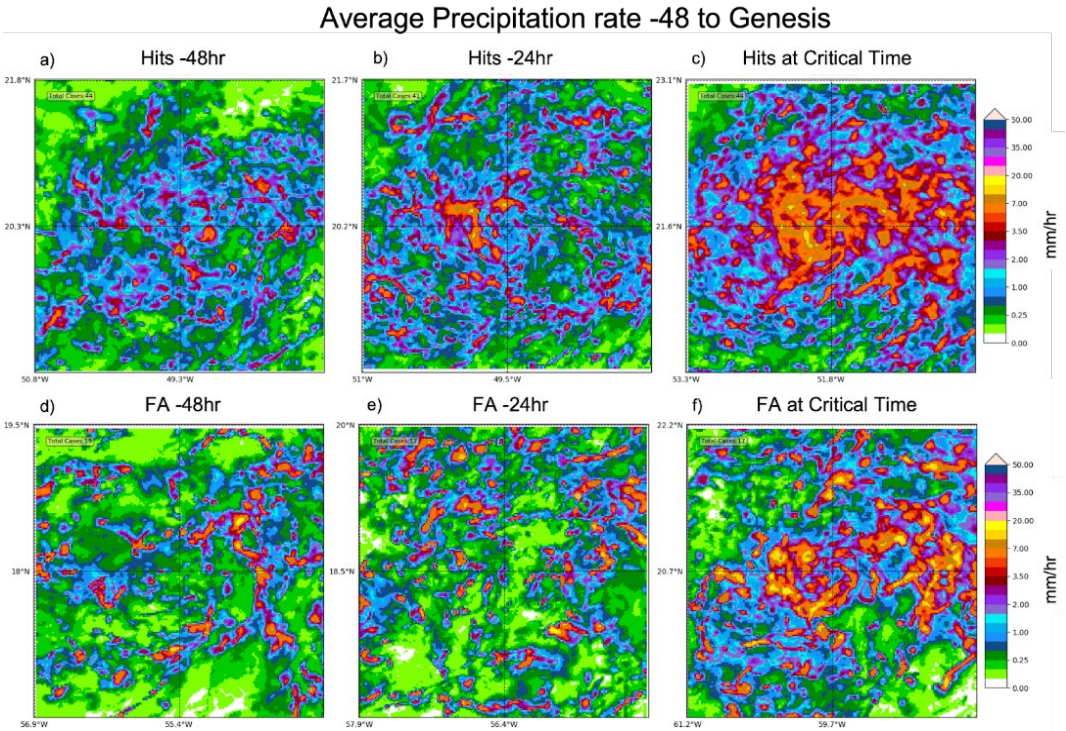

Figure 3. Composite mean precipitation rates (mm/h) for developing disturbances in the North Atlantic from 2017-2020. (a-c) Hits and (d-f) FAs are shown for -48 h (a,d), -24 h (b,e), and 0 h (c,f) relative to the critical time. Each composite is 3°x3° centered on the storm center. Sample sizes are shown on the top left corner of each panel.

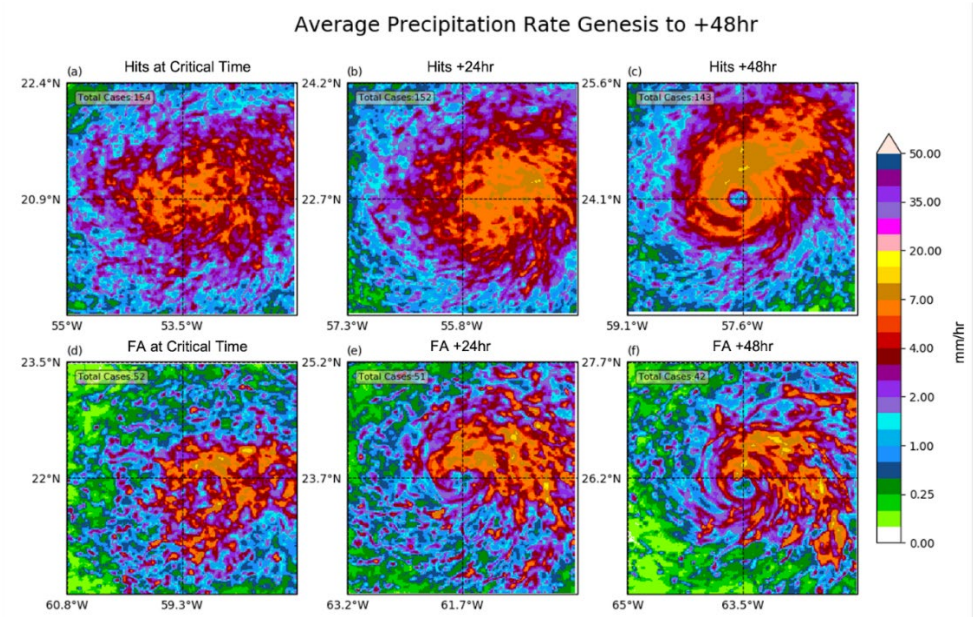

Figure 4. As in Figure 3 but for the critical time (a,d), 24 h (b,e), and 48 h (c,f).

become more symmetrically distributed and intensified in the east and southeast quadrant. The precipitation in the east quadrant acted as a reservoir for TC development. Fritz et al. (2016) also emphasized that heavy precipitation in the southeast quadrant may be associated with the Intertropical Convergence Zone (ITCZ). At +48 h after the critical time, precipitation continued to increase near the eyewall. Nearly the entire eyewall region had precipitation rates > 4 mm h^{-1}. As Ko et al. (2020) mentioned, the highest precipitation occurred near the eyewall where the convection is the strongest. A day after genesis in the false alarm category, maximum precipitation was found to the east and northeast of the circulation. FA rainfall was weaker overall and asymmetrically weighted to the northern semicircle compared with hits. The area of moderate and heavy precipitation rates (> 5 mm h^{-1}) is much larger in the hits composite than in the FA composite. However, at +48 h, eye and eyewall features are apparent in the FA composite, indicating that the TC intensified significantly since genesis, but perhaps not as much as the hits.

3.2.2 Mid-Level Relative Humidity

This section shows results for relative humidity with respect to the critical time at 300 mb, 500 mb, 700 mb, and 850 mb. Figure 5 represents RH at the critical time for the four pressure levels in different events from the contingency table. In the lower troposphere (defined as 850 mb and 700 mb), all the events show high moisture content. In the mid-to-upper troposphere (defined as 500 mb and 300 mb), however, dry air appears in the northwest quadrant for FAs and CNs. The 500 mb RH can be used as an indicator of mid-tropospheric moisture, which has been associated with TC formation in previous studies (Fritz and Wang 2013). As an example, this layer may reflect dry air from the Saharan air

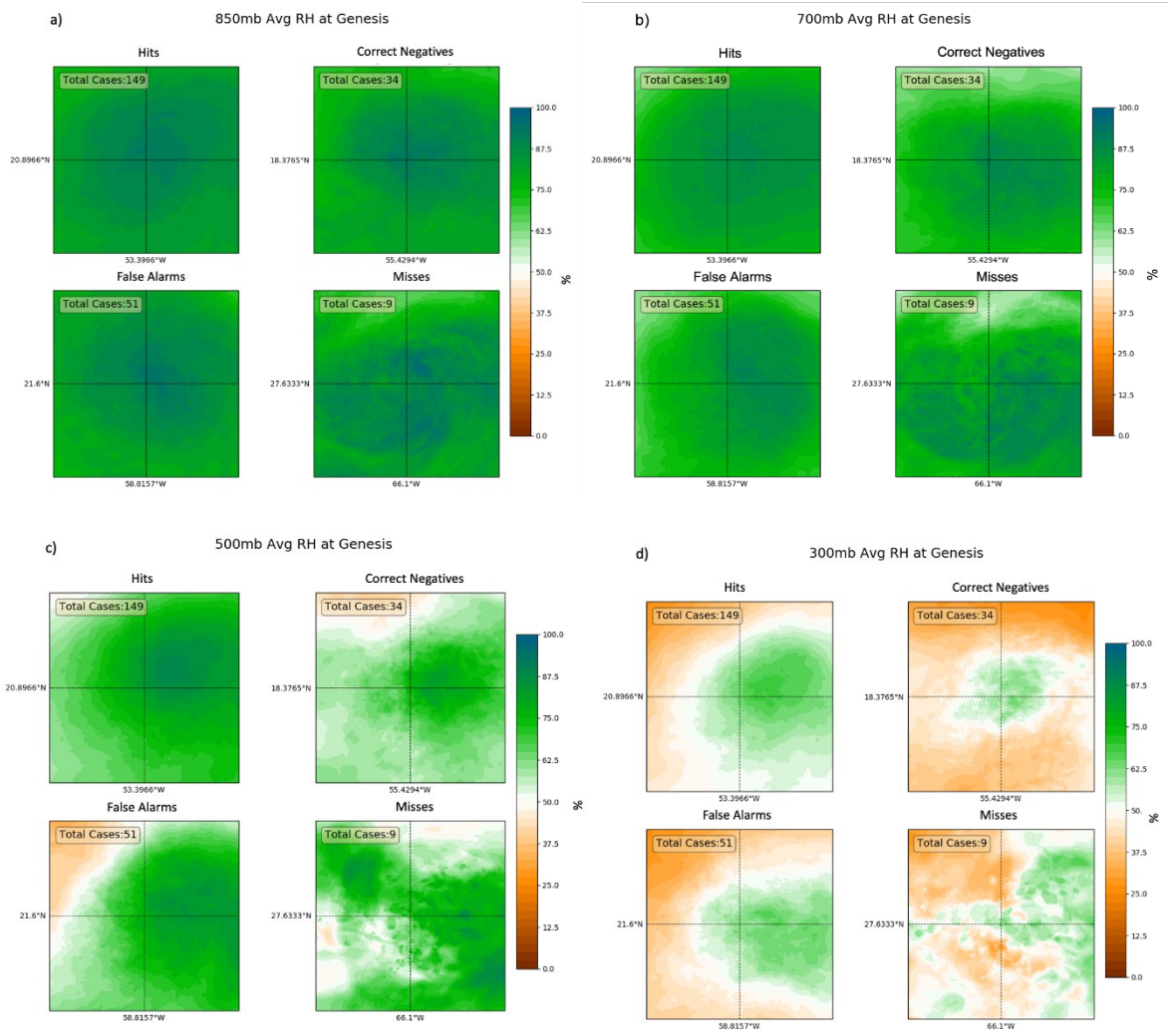

Figure 5. Composite means RH for all the events at the critical time (e.g., Hits, FA, CN, Misses). All the plots are 10°x10° regions centered on the storm center. (a) 850 mb (%), (b) 700 mb RH (%), (c) 500 mb RH (%), (d) 300 mb RH (%). The box on the right represents the location of all the categories.

layer (SAL) as well as mid-latitude dry air intrusions (Dunion 2011). Therefore, 500 mb is selected to evaluate for both developing and non-developing cases.

Abundant moisture is observed near the storm center and in the eastern semicircle, especially the southeast quadrant (Figure 6a-c). RH greater than 50% extends out ~2.5° from the center to the northwest, with a marked decrease in RH to less than 25% at larger radii. By

-24 h, the inner core and eastern semicircle of the storm continues to moisten and the dry zone propagates slowly cyclonically in the outer region of the storm (Figure 6b). It should be noted that the dry air does not advance closer to the storm center leading up to the genesis time. At the critical time (Figure 6c), RH in the inner core and east semicircle exceeds 65% with the maximum RH nearly collocated with the storm center. Importantly, the moisture distribution becomes more symmetric, indicating a thermodynamically favorable environment that is not ventilating the moist inner core with dry environmental air. Although the dry air in the northwest quadrant continues to slowly propagate cyclonically in the outer region of the storm, it also moistened over the preceding 24-h period.

For FA events at -48 h, there is a broad moist region to the east and southeast of the center with a thick layer of dry air in the outer-pouch region (Figure 6d). RH maximizes at least 2° east of the composite center. By -24 h (Figure 6e), the asymmetric moisture structure shifts towards south and southeast. The moist air maximum in the east moves closer to the center, within 2°. The dry air in the north region expands and moves southward. Although at the critical time (Figure 6f) moisture content in the east and southeast increases and moves closer to the center, strong dry air in the north is slowly intruding into the storm vortex. Wu et al. (2015) emphasized that having dry air intrusion into the storm vortex, however, suppresses convection and increases the asymmetry of convection, causing the storm to weaken. Figure 7 shows lead times for Hit and FA cases. The moisture in the hits becomes significantly more symmetric around the center by +48 h, while the air is much drier outside of the center.

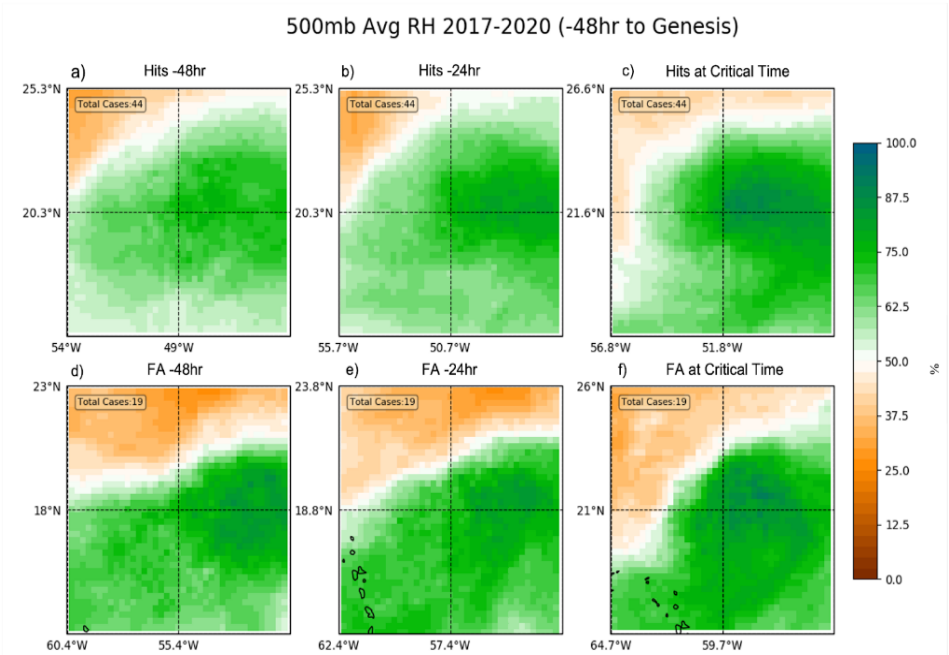

Figure 6. Composite means RH (%) for developing disturbances in the North Atlantic from 2017-2020. (a-c) Hits and (d-f) FAs are shown for -48 h (a,d), -24 h (b,e), and 0 h (c,f) relative to the critical time. Each composite is 10°x10° centered on the storm center. Sample sizes are shown on the top left corner of each plot.

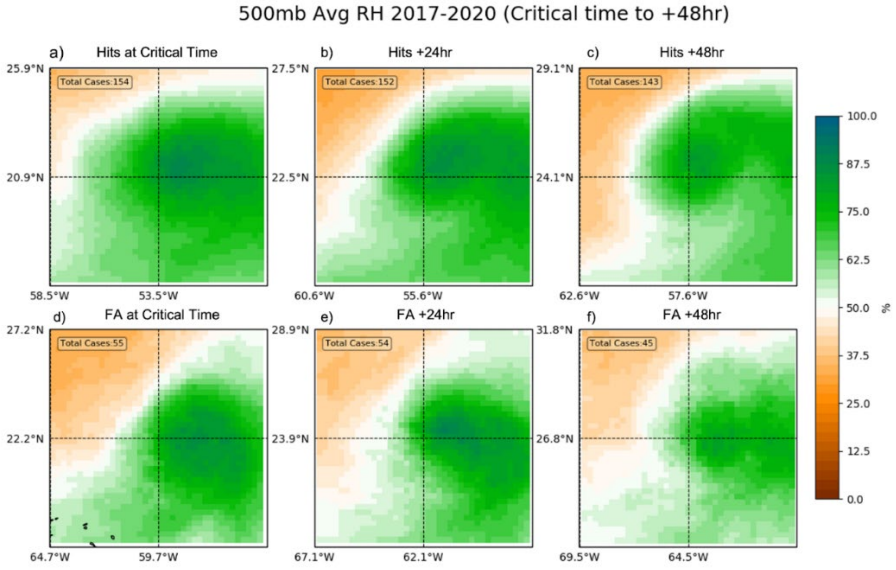

Figure 7. As in Figure 6, but for the critical time (a,d), +24 h (b,e), and +48 h (c,f). FAs, moisture also becomes more symmetrical, but it covers a smaller area than in hits, and it is also notably drier on the west and south sides of the circulation (within 2 degrees).

3.2.3 Vertical Wind Shear

This section analyzes deep vertical wind shear for both Hits and FA. Consistent with previous studies (e.g., Chen et al. 2015), deep-layer VWS is defined as the difference between the 300 mb and 850 mb wind. A lead composite of VWS for hit events is shown in Figure 8a-c. VWS magnitude was low-to-moderate (< 13 m s^{-1}) over the entire 10°x10° region around the storm center in the 48-h period leading up to genesis (i.e., the critical time). It is primarily headed east and southeast. As the system reaches critical time, VWS magnitude decreases slowly near the center and in the southeast and southwest quadrants, with minimum VWS of 5 m s^{-1}. On the other hand, VWS increases gradually in the northeast quadrant. However, this VWS increase is not related to stronger 300 hPa wind (Figure 20a, pg. 43) and is instead attributed to the storm circulation spinning up, especially on the north side. In general, the 300 mb flow decreases over the storm center from 11 m s^{-1} at -48 h to 6 m s^{-1} at the critical time.

In contrast, FA events are typically associated with VWS that are substantially larger than for hit events, especially to the north of the storm (Figure 8d-f). Strong VWS greater than 15 m s^{-1} expands to cover most of the northern semicircle from -48 h to the critical time. At -48 h, the shear magnitude is greater than 15 m s^{-1} in the southeast quadrant. Importantly, VWS increases notably over the storm center, with magnitudes up to 12 m s^{-1} at the critical time (Figure 8f). The VWS direction is comparable to the hit events, but there are some important differences. For example, the VWS vectors reflect more of an anticyclonic shear axis compared with a more classic anticyclone for hit events. This observation is corroborated by

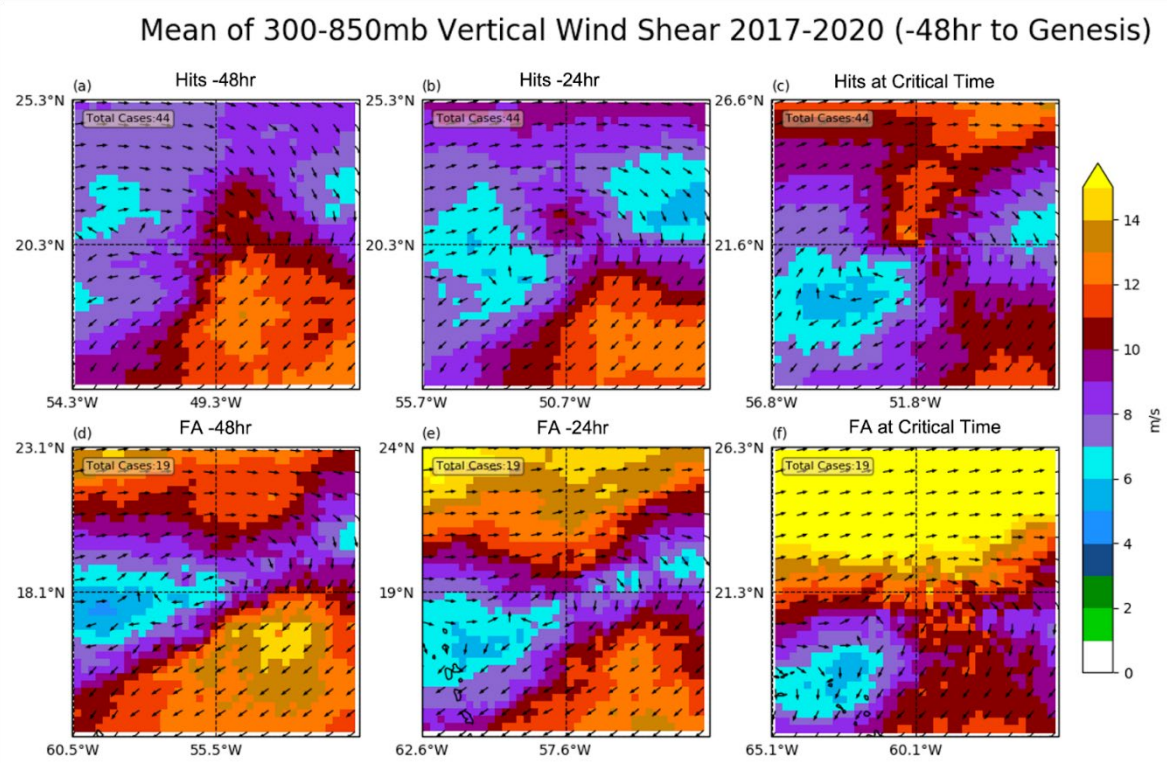

Figure 8. As in Figure 6, except for 300-850 mb VWS (m s^{-1}).

the 300 mb flow, which shows an anticyclone center ~4° east of the storm center (Figure 20b, pg. 43). Previous work (e.g., Hazelton et al. 2022) showed that TCs can develop and intensify along sharp VWS gradients. If VWS predicted by HWRF-B was slightly more favorable (i.e., weaker) than in reality, that could account for the erroneous genesis event. Comparisons with observations will be the focus of future work.

3.3 Non-Developing Cases (Misses, Correct Negatives)

3.3.1 PRECIPITATION RATE

Figure 9d-f shows the composite mean rain rates for CN categories from -48 hours to the critical time. The storm center is surrounded by weak-to-moderate precipitation rates, while areas far from the center receive weaker rates. In Figure 9e, a day before the critical time, moderate precipitation is widely distributed over the entire storm area (i.e., 3°x3° region

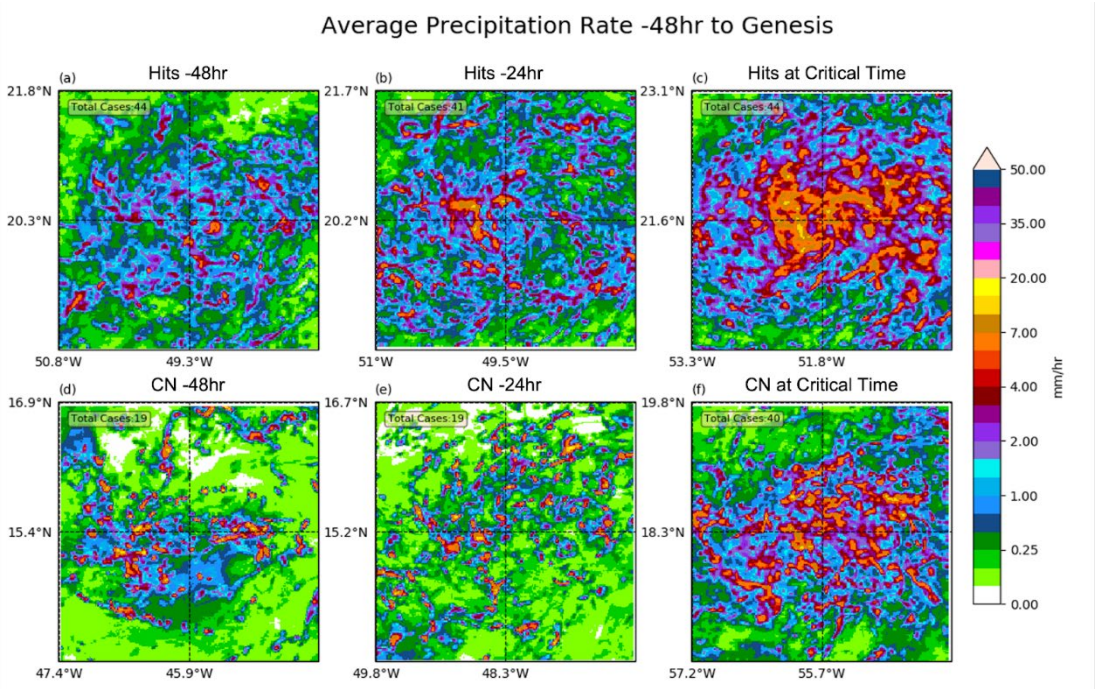

Figure 9. As in Figure 4, except (d-f) show composites for CN events.

centered on the storm). The maximum precipitation rate observed is less than 4 mm h^{-1}. At the critical time, rainfall rates increased substantially in all the quadrants, particularly near the center, as shown in Figure 9f. The model produced significant amounts of light rain in the outer region of the TC. Unlike the CN event, the hits category precipitation rate continuously increased near the center as it reached critical time.

Figure 10d-f represents rainfall rates for Misses from -48 h to the critical time. A weaker and more scattered precipitation distribution is similar to the CN patterns, but the intensity is concentrated near the center. There is an increase in precipitation rate from -48 h to -24 h but it remains widespread and covers fewer area. All the quadrants receive precipitation rates > 4 mm $h^{-1,}$ but it remains scattered at the critical time. In hits and Misses, precipitation rates are higher near the circulation center. Nevertheless, in the hits category, precipitation rates

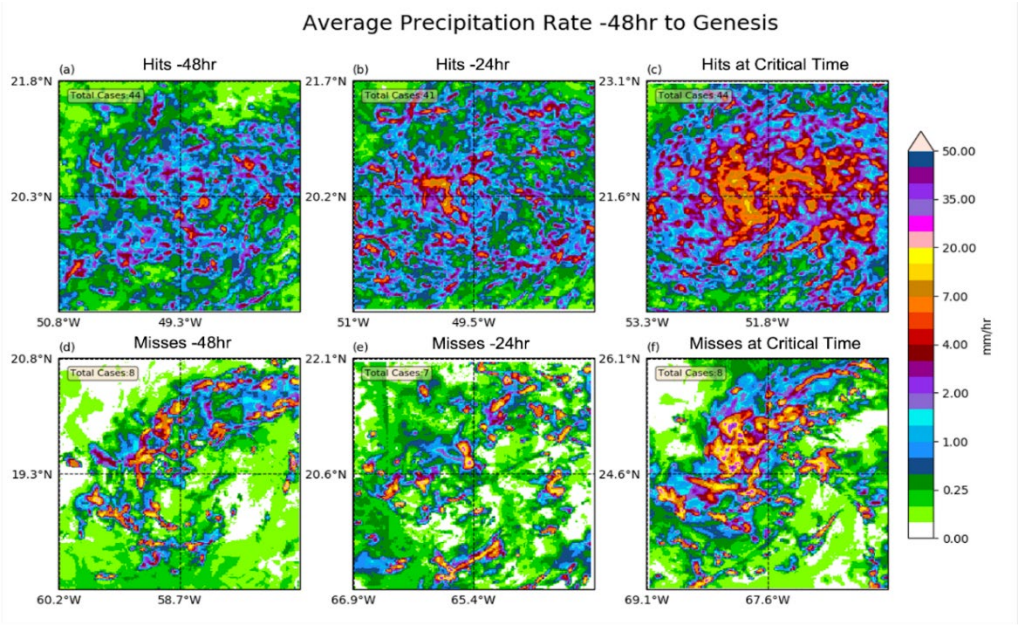

Figure 10. As in Figure 4, except (d-f) show composites for Miss events.

increase as critical time approaches, while in the Misses category, precipitation rates decrease as it reaches Day 0. Previous literature (e.g., Peng et al. 2012) mentioned that precipitation rates increase drastically when TC reaches critical time for developing cases. Figure 11 represents the lag times for both CN and Misses. Precipitation rate continuously decreases in all the quadrants from critical time to Day +2 for CN in Figure 11a-c, indicating that the storm is weakening after it reaches peak intensity. In the Misses (Figure 11d-f), rainfall rates vary throughout its time evolution. It has a period of increasing in the west and northwest quadrants from critical time to +24 h then decreases from +24 h to +48 h. The structure of precipitation rates at +24 h suggests increased convective organization after the time of maximum intensity (i.e., critical time), especially in the northwest quadrant where maximum rates exceed 20 mm h^{-1}. Since the miss events generated into TCs in reality, this result indicates that increasing precipitation rates do not necessarily correlate with TC genesis in HWRF-B forecasts.

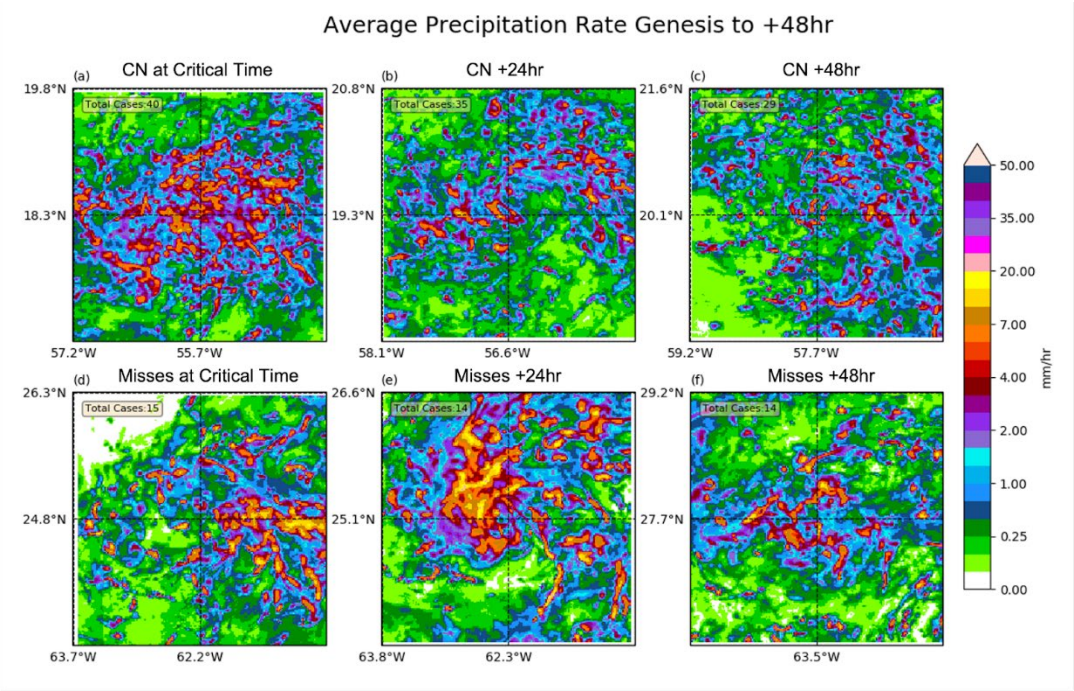

Figure 11. As in Figure 5, except for CN events (a-c) and Miss events (d-f).

3.3.2 Mid-Level Relative Humidity

For CN events, a large area of moist air is present near the circulation at -48 h, but there is also very dry air north and northwest of the storm center (Figure 12d). Moisture near the center gradually increases by -24 h, but dry air also moves within 2° to the storm center (Figure 12e). At the critical time (Figure 12f), the general structure of the moist and dry air remains the same. While RH increases near the center in CN events, relative to Hit events, it covers a smaller area, is elongated in the zonal direction, and has a drier maximum magnitude.

For Miss events at -48 h, moisture is present, but the northwest quadrant is much drier than any of the other event types (Figure 13d). In fact, RH less than 50% is within 1.5° of the storm center at this time. The maximum RH remains constant at -24 h, but the entire region does moisten overall (Figure 13e). At the critical time, dry air reappears to the north of the

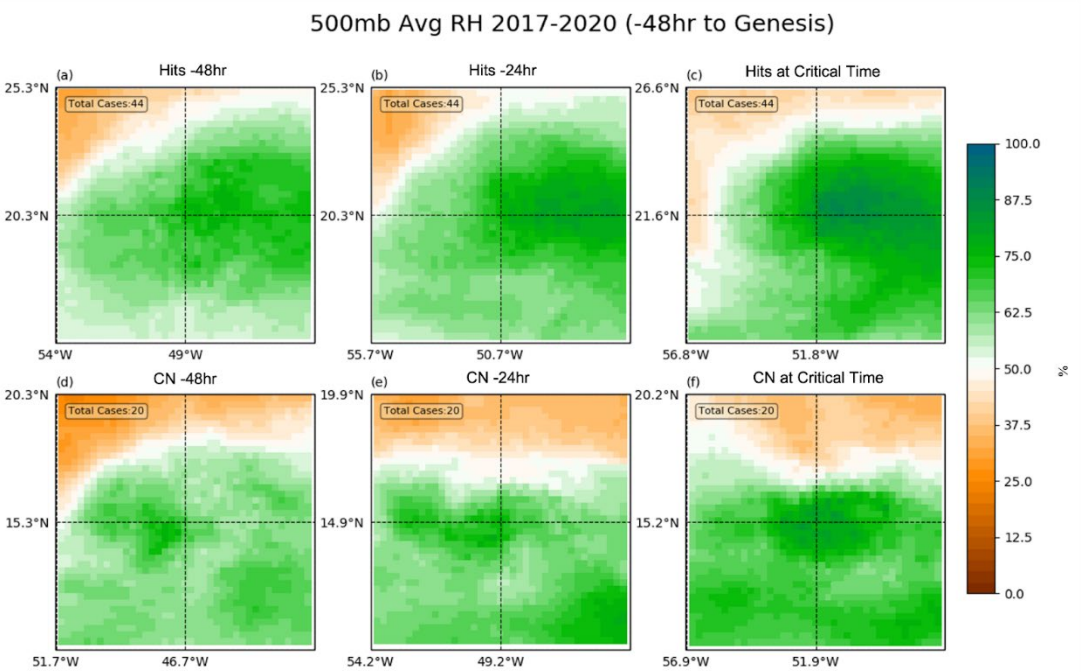

Figure 12. As in Figure 6, except (d-f) show composites for CN events.

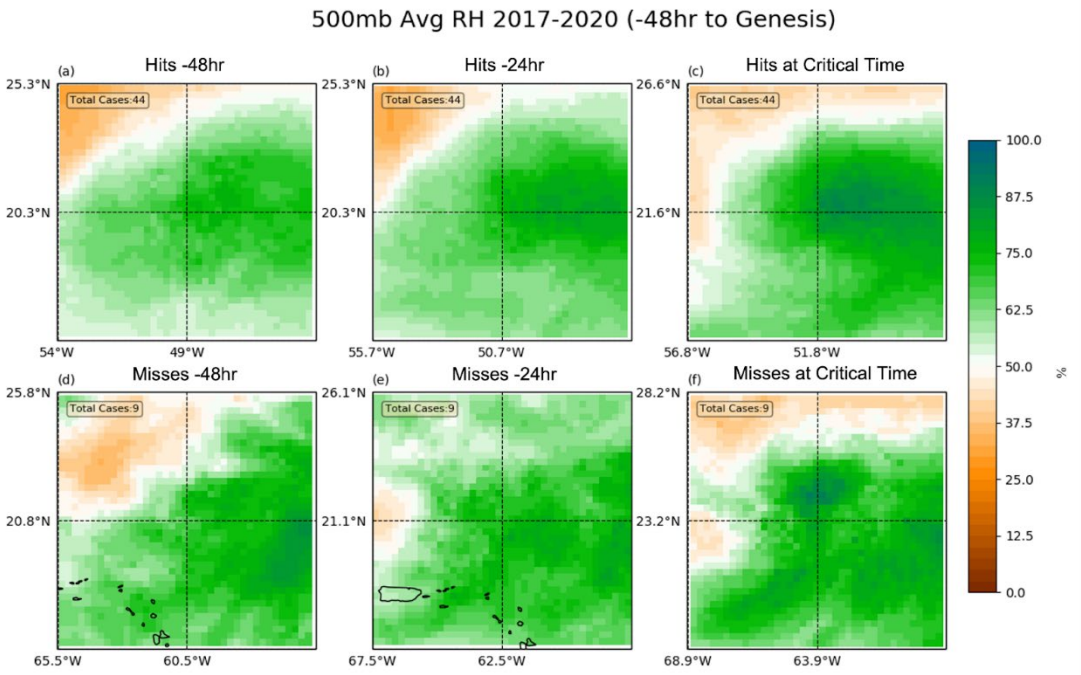

Figure 13. As in Figure 6, except (d-f) show composites for Miss events.

storm center and moisture remains weak and disorganized (Figure 13f). In particular, maximum RH is displaced to the north of the center. For CN, high RH (> 75%) near the center slowly dissipates from the critical time to +48 h (Figure 14a-c). The dry air also diminishes in the north and south of the storm, but persists throughout the evolution. The maximum RH in the lag time for Miss events (Figure 14d-f) gradually decreases, however, the areal coverage increases both to the south and north of the center. Overall, the RH remains weak and disorganized from the critical time to +48 h

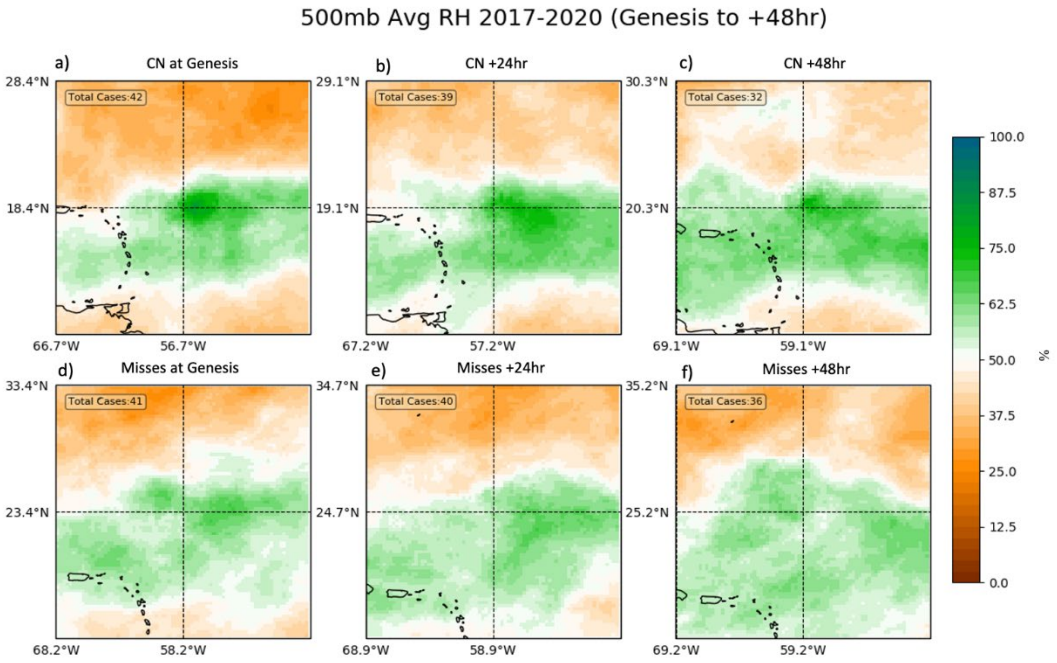

Figure 14. As in Figure 7, except for CN events (a-c) and Miss events (d-f).

3.3.4 Vertical Wind Shear

For CN cases, VWS increases near the center from -48 h to -24 h, but decreases from -24 h to critical time in the east and southeast quadrants (Figure 15d-f). North and northwest quadrants show slow increase and expansion of VWS, but magnitude remains relatively low

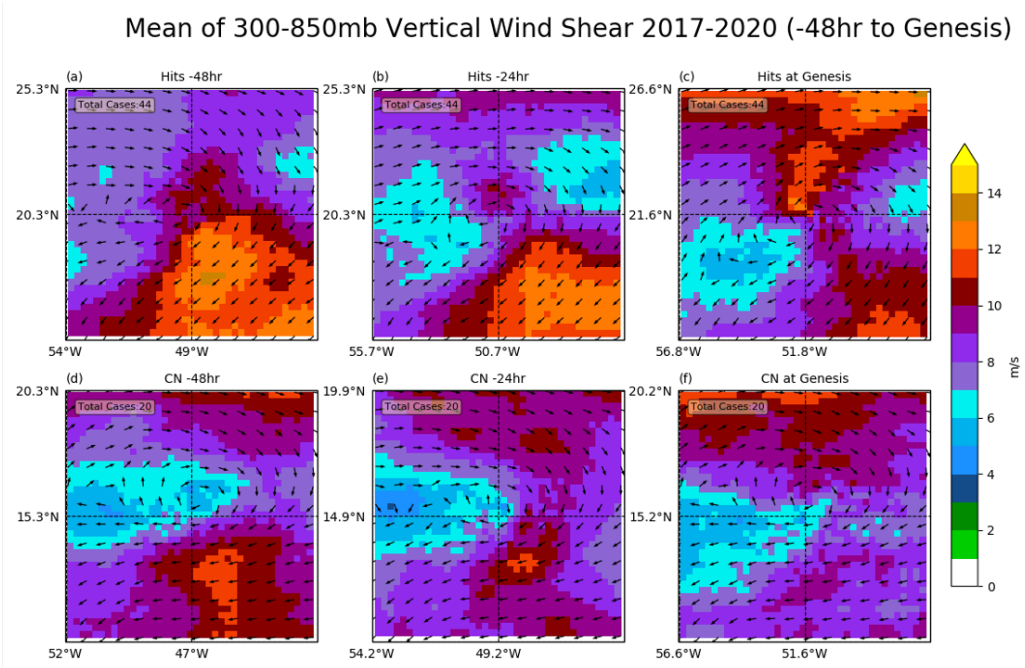

Figure 15. As in Figure 8, except (d-f) show composites for CN events.

(< 12 ms^{-1}). Low-to-moderate VWS was present in both Hits and CN throughout the analysis period. VWS did increase in CN from -48 h to -24 h, but values remained within a moderate range. For Miss events, VWS behaves similarly to the hits cases as the system reaches critical time, with the shear magnitude decreasing slowly in the southeast quadrant and gradually increasing in the northeast quadrant (Figure 16d-f). However, VWS gradually increased near the center as hits present lower values in the circulation region.

3.4 Quantitative Analyses

3.4.1 Multiple Proxies for Analyzing Precipitation

Using two proxies, we were able to analyze the thermodynamic properties of developing and non-developing cases. Figure 17 illustrates a time series of the maximum precipitation rate for all event types. These results qualitatively represent what we observed in the

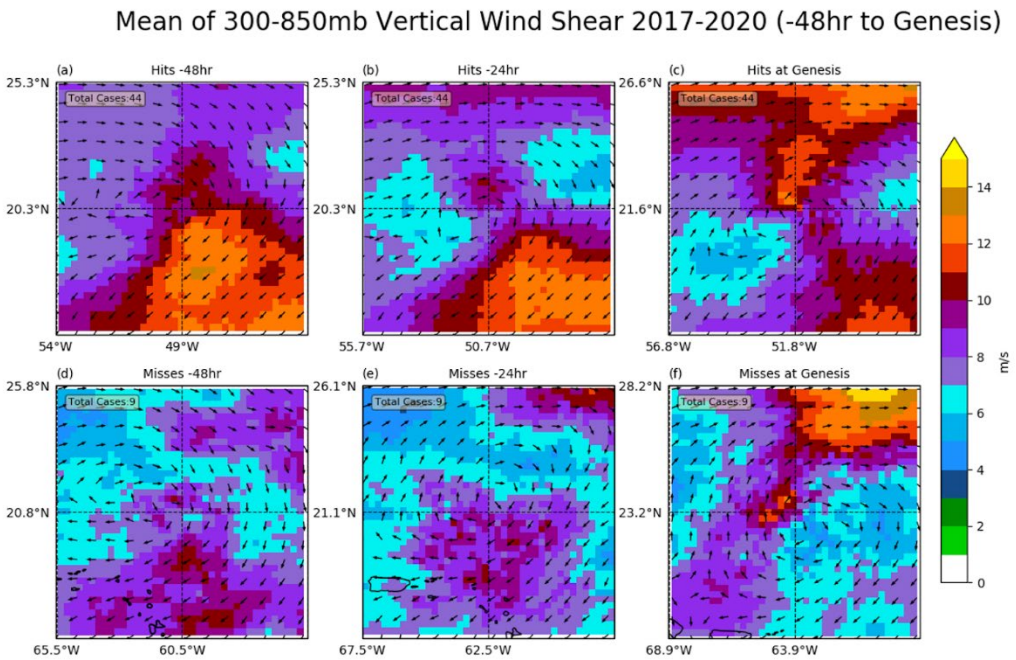

Figure 16. As in Figure 8, except (d-f) show composites for Miss events.

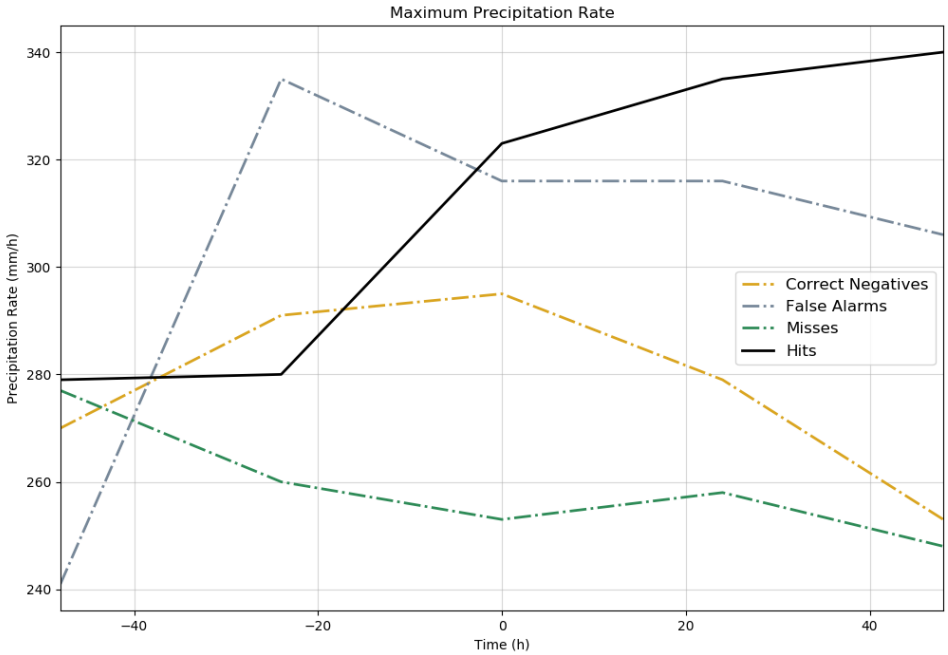

Figure 17. Composite maximum precipitation rate (mm h^{-1}) for all the events from -48 h to +48 h.

composite precipitation rate plots. Recall that precipitation rates are instantaneous, and, therefore, maximum values can be quite high. For hit events, the precipitation rate is constant between -48 h and -24 h. However, from -24 h to the critical time, the maximum rate increases to over 320 mm h^{-1}. The precipitation rate continued to increase at positive hours, indicating further convective organization that is supported by Figure 4c. From Figure 4d-f, there is no indication that the precipitation rate spiked suddenly before the critical time for FA events. However, the maximum precipitation rate substantially increases from ~240 mm h^{-1} at -48 h to over 330 mm h^{-1} at -24 h before declining to under 320 mm h^{-1} as the critical time. The surge in maximum precipitation rate at -24 h might indicate convection in FA events that was overactive compared with reality. However, despite the high maximum rate at -24 h, the precipitation was quite scattered (see Figure 4e). The evolution of maximum precipitation rates for CN and Misses may be viewed as mirror images of one another (Figure 17). Both event types are initially similar (270-280 mm h^{-1}). However, the CN rate increases to near 290 mm h^{-1} at the critical time. After the critical time, the maximum rate decreases to near 250 mm h^{-1}. Conversely, for Miss events, maximum precipitation rates actually decrease from -48 h to the critical time (~250 mm h^{-1}). This evolution supports non-development in the model, but it suggests that precipitation rates were overall too weak to support TC genesis. The results clearly show that maximum precipitation rates are higher for developing events than for non-developing events.

As another thermodynamic proxy, the percent coverage of different precipitation thresholds was calculated for all event types to analyze rain rate. Overall, Figure 18, shows that the precipitation rate increases for all the thresholds and all event types leading up to the

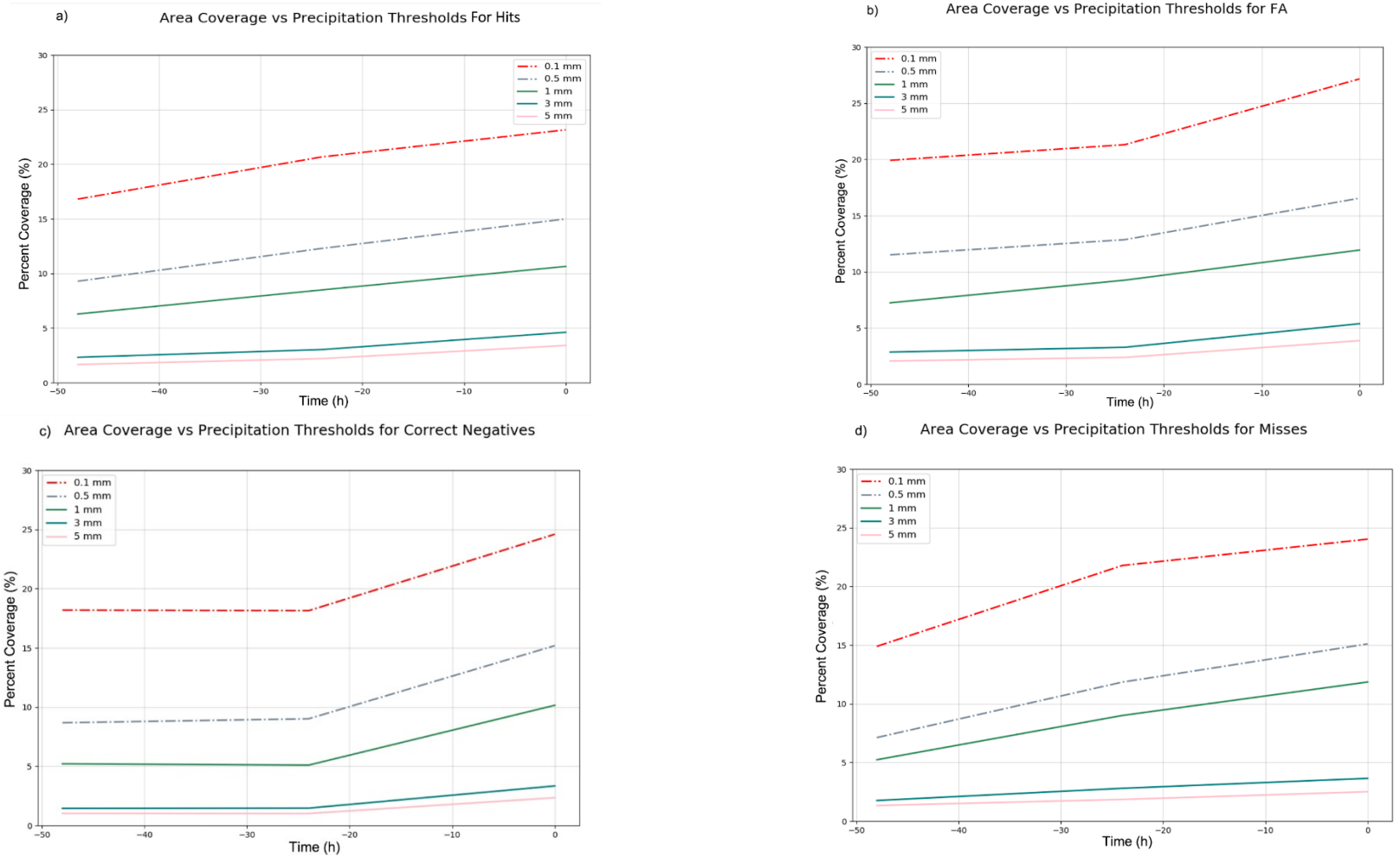

Figure 18. Percent coverage for different precipitation rate (mm/h) thresholds separated by event type. y-axis shows Percent coverage (%) and x-axis display -48 h to the critical time. (a-d) represent Hits, FA, CN, Misses respectively. Dashed red line (≤ 0.1 mm), dashed cyan line (0.1 mm ≥ and ≤ 0.5 mm), solid green line (0.5 mm ≥ and ≤ 1 mm), solid light gray line (1 mm ≥ and ≤ 3 mm), solid teal line (3 mm ≥ and ≤ 5 mm).

critical time. The percent coverage of rain rates greater than or equal to 1 mm h^{-1} is larger for developing cases than for non-developing disturbances as genesis nears. Even two days prior to genesis, FA shows a higher percent coverage for more intense rainfall than in the non-developing cases. Precipitation rates increase in area coverage for both CN and FA events from 1 day before genesis, though FA has a larger total raining area across all the thresholds. The results for increasing trend in percent coverage of stronger precipitation are consistent with those obtained by Wang (2018) and Fritz et al. (2016) who both showed an increase in areal coverage of convection within -36 h to -12 h of genesis in the Atlantic basin. Although we did not explicitly examine different precipitation types, high rain rates are typically associated with deep convection (e.g., Wang 2018).

3.4.2 Analyzing Relative Humidity

Figure 19 represents moisture differences between Hits and the other three event types from the contingency table (Figure 2). RH differences reveal interesting patterns that separate Hit events from the other event types. Compared with FA events, Hit events have higher mid-tropospheric RH to the north of the center at all lead times and have higher RH to the west of the center at the critical time (Figure 19a). Higher RH to the west of the center prior to genesis could reduce the entrainment of dry air into the developing vortex. Higher VWS for FA events supports the advection of drier environmental air closer to the storm center. Compared with CN events, Hit events have higher RH to the north and east of the center at all lead times (Figure 19b). Drier conditions in CN events could be linked with higher-amplitude SAL events. Compared with Miss events, Hit events have higher mid-tropospheric RH generally to the north of the center (Figure 19c). However, the relatively small

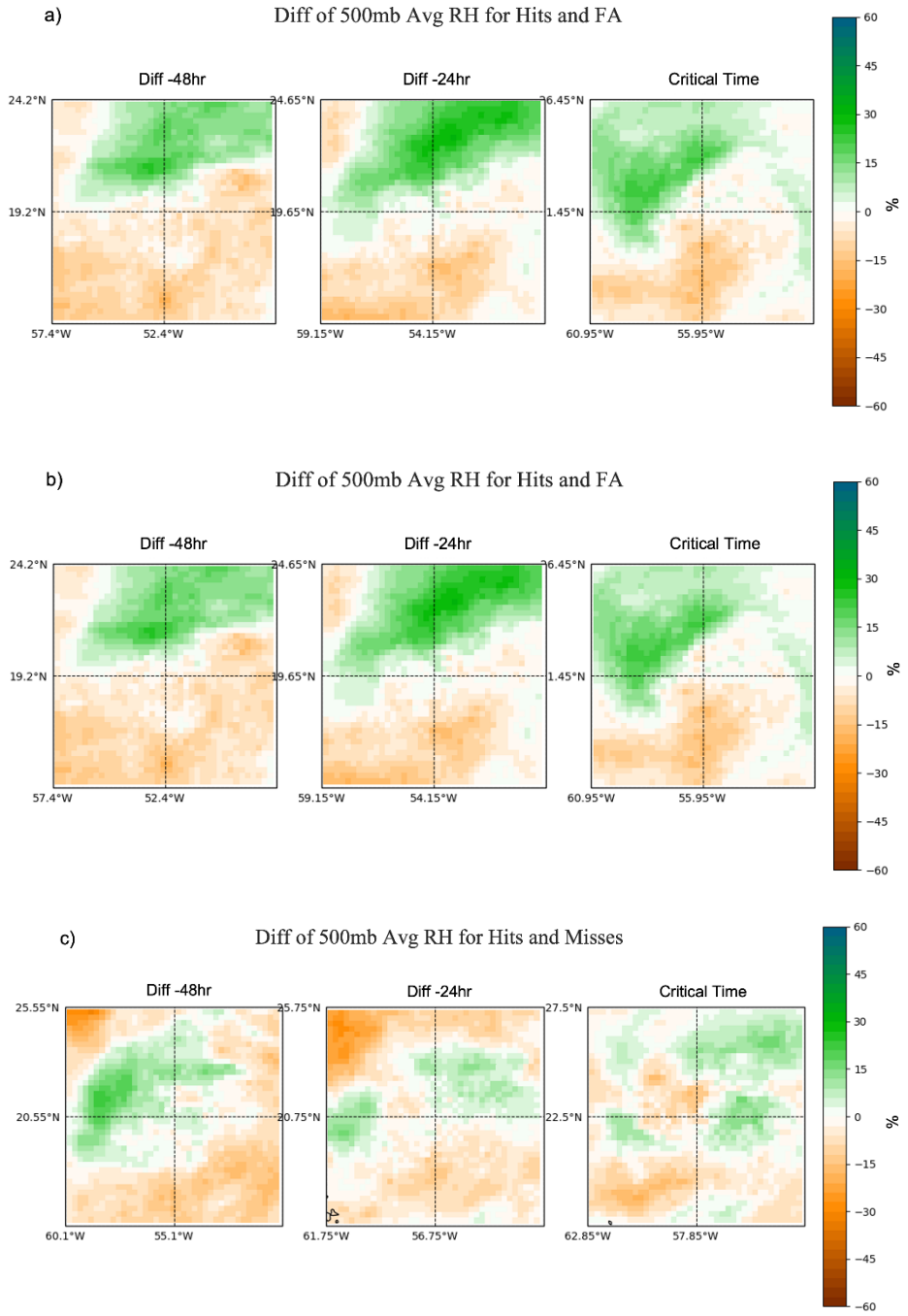

Figure 19. (a) Hits and FA RH (%), (b) Hits and CN RH (%), (c) Hits and Misses RH (%).

differences at -24 h and the critical could indicate a similar environment for these events that experienced TC genesis in reality. The larger differences at -48 h indicate that M events are notably drier, especially to the west and north. This dry air may have reduced TC genesis probability by delaying the moistening process that is key to TC genesis. Compared to Peng et al. (2012), this result differs from their claim that developing disturbances have a higher relative humidity at 500 hPa than non-developing disturbances. In fact, FA events, which developed in the model, have the lowest RH in the northwest quadrant of any event type. These results indicate that Hit events have a unique moisture evolution, with notable differences from the other event types in the northern semicircle. In general, higher RH in this region is related to the HWRF-B model correctly predicted TC genesis.

3.4.3 Analyzing VWS

Our final metric was plotting the deep VWS for all events. It has been shown in many previous studies that TC formation is enhanced by the absence or very mild presence of shear. In a high VWS environment, failed TC genesis occurs because the vortex is continually prevented from aligning vertically and because dry air is typically advected into the storm circulation. As a result of high VWS, convection is often displaced from the storm center, thus preventing a decrease in surface pressure and a more intense deep convection. It was, however, demonstrated in our study that non-developing disturbances were, on average, characterized by weak deep-layer VWS before and at the critical time. Peng et al. (2012) showed that developing cases can have higher VWS values than non-developing cases. Our study evaluated the 300 mb flow to understand its contribution to VWS (Figure 20). In general, strong upper-tropospheric flow is detrimental to TC genesis. Additionally, upper-

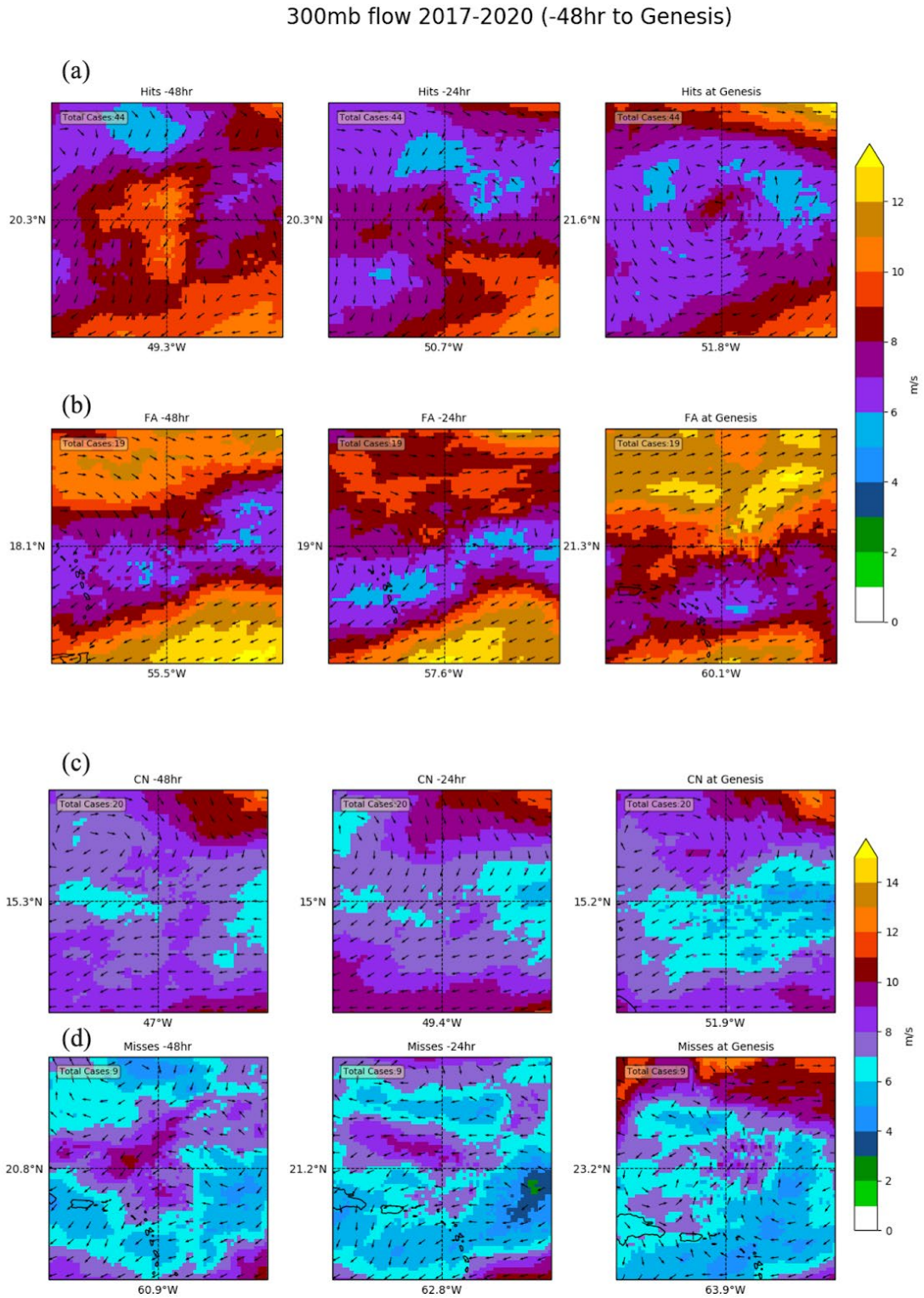

Figure 20. Composite 300mb flow for all the events. (a) Hits, (b) FA, (c) CN, (d), Misses.

level winds could enhance storm outflow, and, consequently, TC genesis, when the flow is weak or is characterized by divergence. Favorable upper-tropospheric winds support deep convection. It has been acknowledged by Hazelton et al. (2022) that outflow can "push back" against large-scale shear and provide protection for the TC core. For Hit events, upper-level flow quickly organizes into an upper-level anticyclone that reflects healthy outflow (Figure 20a). For FA events, the 300 mb winds reveal an anticyclonic shear axis, with a closed anticyclone to the east of the storm center at the critical time (Figure 20b). Non-developing cases exhibit weaker outflow and weaker anticyclonic vorticity (Figure 20c,d). In general, developing cases have anticyclonic upper-tropospheric flow and non-developing cases do not have favorable set up. Another key difference between developing (Figure 20a,b) and non-developing (Figure 20c,d) events is the direction of the 300 mb flow; non-developing events have a noticeable easterly component to the flow. Consequently, there is less dynamic support for convection and storm intensification. Furthermore, it is critical to note that strong upper-level outflow must be located in the "sweet spot", i.e., not too close to the center that it impacts the core, but not too far away that it not influence convection. This can be observed in both Hit and FA events (Figure 20a,b).

4. Conclusions

This study focused on the evaluation of TC genesis forecasts in a high-resolution NWP model for hurricanes. Specifically, three points were investigated using the Basin-scale Hurricane Weather Research and Forecasting (HWRF-B) model: 1) the performance of TC genesis forecasts, 2) the relationship between precipitation evolution and TC genesis, and 3) the impact of the synoptic-scale environment on precipitation in both developing and non-developing cases. Previous studies have analyzed the influence of thermodynamics and dynamics on precipitation and TC genesis (i.e., tropical cyclogenesis) in NWP models. This study, however, employs an advanced, high-resolution, non-idealized model that has been shown to improve multi-scale and multi-storm interactions and, subsequently, TC forecasts (Alaka et al. 2022). Given the importance of multi-scale interactions for TC genesis, HWRF-B was an attractive option for this study. The HWRF-B model was run for pre-TC disturbances that were identified by the NHC as "invests". Upon meeting our genesis definition, the invest forecasts were then classified as developing or non-developing. By comparing with the NHC best track, each HWRF-B forecast was categorized as a hit, false alarm (FA), correct negative (CN), or Miss. A critical time was defined to create lead/lag composites for each event type. For developing cases, the critical time is defined as the first forecast hour for which the maximum 10-m wind speed is greater than or equal to 34 knots for 12 consecutive hours. For non-developing cases, the critical time is defined as the first forecast hour that the maximum 10-m wind speed is reached. A five-day time window centered on the critical time (i.e., from 2 days before to 2 days after) was composited for each type of event.

Our results showed that the precipitation rates for developing disturbances are significantly higher than those for non-developing disturbances even -48 h before genesis. Rainfall rates continuously increased and covered a broader area leading up to the critical time in developing cases; however, precipitation rates did not increase in a straightforward manner in non-developing cases (Figures 17-18). For example, the area coverage of precipitation rates in CN events did not increase prior to the critical time, and the maximum precipitation rate in Miss events actually decreased before the critical time. In general, intense precipitation rates are greater in the center of developing disturbances (see Figure 3). This is more clear within 1° of the storm center. These figures together emphasize the importance of having a larger raining area from -24 h to the critical time and more intense precipitation closer to the storm center for genesis to occur. This is in agreement with previous studies that precipitation rate increases sharply from -24 h to the critical time in the developing cases (Wang and Hankes 2016; W. Zhang et al. 2015). As Wang (2018) mentioned, heavy precipitation associated with deep convection can force the secondary circulation and low-level vorticity. Thus, HWRF-B forecasts of rainfall for pre-TC events are consistent with the literature and can potentially provide guidance on the fate of invests.

Hit events have higher moisture content in and around the circulation center compared to other events. In particular, FA, CN, and Miss events were characterized by drier air in the northern semicircle of the circulation that persisted throughout the evolution. In the FA events, dry air wrapped cyclonically and inward toward the center by the critical time. A study by Wu et al. (2015) emphasized that dry air intrusion could result in the weakening of a TC as it induces asymmetric convection. Although Hit events showed greater RH compared

to the other cases, FA which developed in the model had similar moisture to the CN category. The outcome from this result suggests that the evolution of RH is an adequate proxy to distinguish between non-developing and developing disturbances in reality. Many studies have suggested that substantial vertical wind shear (VWS) is detrimental to TC formation. The result from this study shows a more nuanced relationship between VWS and TC genesis. Surprisingly, non-developing disturbances also had weak upper-level flow and weak VWS, with Miss events characterized by the weakest flow and VWS. In contrast, FA events exhibited the strongest VWS and 300 mb flow, calling into question the resilience of the vortex in HWRF-B. However, Miss events were much drier than other events in the upper troposphere (300 mb), and this drier air might have reduced deep convection and prevented TC genesis (Figure 5). Future work will investigate if the upper troposphere was too dry in Miss events compared to observations. Also, when comparing the evolution of precipitation rate between developing and non-developing cases, the developing cases had greater maximum precipitation rates and larger area coverage of higher precipitation rates at most lead/lag times than the non-developing cases (see Figure 17). In Hit events, the thermodynamic environment appears to be more important than the dynamic environment, as evidenced by ample moisture and higher-than-expected VWS. However, the fact that FA events become TCs despite higher VWS than and similar RH to non-developing cases is a confusing result that suggests the importance of the model initial conditions. In non-developing cases, moisture before the critical time, especially 48 h prior, was reduced compared to Hit events, reflecting a drier environment that did not support TC genesis.

One of the main objectives of this study was to understand the interaction of multiple environmental factors that affect genesis (e.g., VWS, RH). It is apparent from the results of the developing events that internal processes play a significant role in the formation of TC. As discussed earlier, an increase in intense precipitation prior to genesis indicates the presence of deep convection within the inner core region. Deep convection can be sustained by gradual moistening of the low-to-mid troposphere. Convection in the humidified inner core moistens the upper troposphere and spins up the low-level circulation. It is apparent from Figure 5d that deep convection moistens the upper-level troposphere in developing cases. In the case of FA, perhaps the mid-level vortex generated by deep convection near the center maintains moisture and a healthy structure to prevent the entry of dry air even with the presence of strong VWS. In non-developing cases, the inner core region does not appear to be completely covered by high moisture or intense precipitation. There may be a reduction in secondary circulation strength and a weakening of vortex precession as convection is advected farther away from the low-level center.

5. Future Work

While this study has investigated the relationship between thermodynamic and dynamic variables to TC genesis, much still remains to be learned about the specific pathway(s) to genesis and how that compares with observations. For instance, precipitation can be classified into three types (e.g., stratiform, mid-level convection, and deep convection) which will give us a better understanding of how precipitation type leads to TC genesis. Additionally, it would be beneficial to compute the moisture budget for the HWRF-B model and evaluate its relationship with precipitation and TC formation. Wang et al. (2017) study provided a simple method to calculate the moisture by separating it into moisture transport and surface evaporation. Furthermore, converting the current coordinate system to polar-cylindrical will improve the clarity of previous plots and help quantify the results. For instance, Ko et al. (2020), calculated the radial distribution of mean rain rate for hurricane Harvey. A range of radiuses from the storm center can be used to determine the location of heavy or weak precipitation. Furthermore, to fully understand the differences between developing and non-developing cases, we need to apply statistical analysis. An example might be calculating the domain average of VWS or the average maximum wind at different forecast times. Finally, the model performance should be verified against observational data which are assumed as truth for rainfall amounts. However, since TC genesis occurs over the ocean, there are limited observations available that provide rainfall amounts. Reanalysis (e.g., ECMWF Re-Analysis) and analysis (e.g., GFS analysis can provide a best guess of observations in data sparse regions).

REFERENCES

Agudelo, P. A., C. D. Hoyos, J. A. Curry, and P. J. Webster, 2011: Probabilistic discrimination between large-scale environments of intensifying and decaying African Easterly Waves. *Climate Dyn*., **36**, 1379–1401, https://doi.org/10.1007/s00382-010-0851-x.

Alaka, G. J., Jr., and E. D. Maloney, 2012: The influence of the MJO on upstream precursors to African easterly waves. *J. Climate*, **25**, 3219–3236, https://doi.org/10.1175/JCLI-D-11-00232.1.

Alaka, G. J., Jr., D. Sheinin, B. Thomas, L. Gramer, Z. Zhang, B. Liu, H.-S. Kim and A. Mehra, 2020: A hydrodynamical atmosphere/ocean coupled modeling system for multiple tropical cyclones. *Atmos.*, **11**, 869, https://doi.org/10.3390/atmos11080869.

Alaka, G. J., Jr., X. Zhang, and S. G. Gopalakrishnan, 2022: High-definition hurricanes: Improving forecasts with storm-following nests. *Bull. Amer. Meteor. Soc.*, **103**, E680-E703, https://doi.org/10.1175/bams-d-20-0134.1.

Ashraf, S. M., 2019: *Structural Building Design: Wind and Flood Loads*. CRC Press, 178 pp.

Atlas, R., V. Tallapragada, and S. Gopalakrishnan, 2015: Advances in tropical cyclone intensity forecasts. *Mar. Technol. Soc. J*., **49**, 149–160, https://doi.org/10.4031/MTSJ.49.6.2.

Avila, L. A., and R. J. Pasch, 1992: Atlantic tropical systems of 1991. *Mon. Wea. Rev*., **120**, 2688–2696, https://doi.org/10.1175/1520-0493(1992)120<2688:ATSO>2.0.CO;2.

Avila, L. A., R. J. Pasch, and J. Jiing, 2000: Atlantic tropical systems of 1996 and 1997: Years of contrasts. *Mon. Wea. Rev*., **128**, 3695–3706, https://doi.org/10.1175/1520-0493(2000)128<3695:ATSOAY>2.0.CO;2.

Bao, J., G. Gopalakrishnan, S. G. Michelson, and M. T. Montgomery, 2012: Impact of physics representations in the HWRFX on simulated hurricane structure and pressure–wind relationships. *Mon. Wea. Rev*., **140**, 3278–3299, https://doi.org/10.1175/MWR-D-11-00332.1.

Bentley, A. M., L. F. Bosart, and D. Keyser, 2017: Upper-tropospheric precursors to the formation of subtropical cyclones that undergo tropical transition in the North Atlantic basin. *Mon. Wea. Rev*., **145**, 503–520, https://doi.org/10.1175/MWR-D-16-0263.1.

Beven, J. L., 1999: The boguscane—A serious problem with the NCEP medium range forecast model in the Tropics. *Preprints, 23rd Conf. on Hurricanes and Tropical Meteorology,* Dallas, TX, Amer. Meteor. Soc. Vol. 845.

Blake, E. S., and D. A. Zelinsky, 2018: Hurricane Harvey. National Hurricane Center Tropical Cyclone Report, https://www.nhc.noaa.gov/data/tcr/AL092017_Harvey.pdf.

Biswas, M. K., and Coauthors, 2018a: Hurricane Weather Research and Forecasting (HWRF) Model: 2017 Scientific Documentation. No. NCAR/TN-544+STR, 111 pp, http://dx.doi.org/10.5065/D6MK6BPR.

Biswas, M. K., L. Carson, K. Newman, D. Stark, E. Kalina, E. Grell, and J. Frimel, 2018b: Community HWRF users' guide V 4.0 a. NCAR Tech. Note, 162 pp, https://dtcenter.org/sites/default/files/community-code/hwrf/docs/users_guide/HWRF-UG-2018.pdf.

Biswas, M. K., D. Stark, and L. Carson, 2018c: GFDL Vortex Tracker Users' Guide V3.9a, 35 pp.

Chen, Q., J. Fan, S. Hagos, W. I. Gustafson Jr., and L. K. Berg, 2015: Roles of wind shear at different vertical levels: Cloud system organization and properties. *J. Geophys. Res. Atmosph.*, **120**, 6551–6574, https://doi.org/10.1002/2015jd023253.

Davis, C. A., and Coauthors, 2008: Prediction of landfalling hurricanes with the Advanced Hurricane WRF model. *Mon. Wea. Rev*., **136**, 1990–2005, https://doi.org/10.1175/2007mwr2085.1.

Dong, J., and Coauthors, 2020: The evaluation of real-time Hurricane Analysis and Forecast System (HAFS) Stand-Alone Regional (SAR) model performance for the 2019 Atlantic hurricane season. *Atmos*., **11**, 617, https://doi.org/10.3390/atmos11060617.

Dunion, J. P., 2011: Rewriting the climatology of the tropical North Atlantic and Caribbean Sea atmosphere. *J. Climate*, **24**, 893–908, https://doi.org/10.1175/2010jcli3496.1.

Elsberry, R. L., L. Chen, J. Davidson, R. Rogers, Y. Wang, and L. Wu, 2013: Advances in understanding and forecasting rapidly changing phenomena in tropical cyclones. *Tropical Cyclone Res. Rev.*, **2**, 13-24, https://doi.org/10.6057/2013TCRR01.02.

Enyew, B. D., and A. Mekonnen, 2022: The interaction between African easterly waves and different types of deep convection and its influence on Atlantic tropical cyclones. *Atmos.*, **13**, 5, https://doi.org/10.3390/atmos13010005.

Frank, W. M., and P. E. Roundy, 2006: The role of tropical waves in tropical cyclogenesis. *Mon. Wea. Rev*., **134**, 2397–2417, https://doi.org/10.1175/mwr3204.1.

Fritz, C., and Z. Wang, 2013: A numerical study of the impacts of dry air on tropical cyclone formation: A development case and a nondevelopment case. *J. Atmos. Sci*., **70**, 91–111, https://doi.org/10.1175/JAS-D-12-018.1.

Fritz, C., Z. Wang, S. W. Nesbitt, and T. J. Dunkerton, 2016: Vertical structure and contribution of different types of precipitation during Atlantic tropical cyclone formation as revealed by TRMM PR. *Geophys. Res. Lett.*, **43**, 894–901, https://doi.org/10.1002/2015GL067122.

Galarneau, T. J., R. McTaggart-Cowan, L. F. Bosart, and C. A. Davis, 2015: Development of North Atlantic tropical disturbances near upper-level potential vorticity streamers. *J. Atmos. Sci.*, **72**, 572–597, https://doi.org/10.1175/jas-d-14-0106.1.

Gall, R., J. Franklin, F. Marks, E. N. Rappaport, and F. Toepfer, 2013: The hurricane forecast improvement project. *Bull. Amer. Meteor. Soc*., **94**, 329–343, https://doi.org/10.1175/BAMS-D-12-00071.1.

Gopalakrishnan, S., and Coauthors, 2020: 2019 HFIP R&D activities summary: Recent results and operational implementation. NOAA HFIP Tech. Rep. HFIP2020-1, 42 pp, https://hfip.org/sites/default/files/documents/hfip-annualreport-fy2019.pdf.

Gopalakrishnan, S., S. Goldenberg, T. Quirino, X. Zhang, F. D. Marks Jr., K.-S. Yeh, R. Atlas, and V. Tallapragada, 2012: Toward improving high-resolution numerical hurricane forecasting: Influence of model horizontal grid resolution, initialization, and physics. *Wea. Forecasting*, **27**, 647–666, https://doi.org/10.1175/WAF-D-11-00055.1.

Gopalakrishnan, S., F. Marks Jr., X. Zhang, J.-W. Bao, K.-S. Yeh, and R. Atlas, 2011: The experimental HWRF system: A study on the influence of horizontal resolution on the structure and intensity changes in tropical cyclones using an idealized framework. *Mon. Wea. Rev.*, **139**, 1762–1784, https://doi.org/10.1175/2010mwr3535.1.

Gopalakrishnan, S., F. Marks, J. Zhang, X. Zhang, J.-W. Bao, and V. Tallapragada, 2013: A study of the impact of vertical diffusion on the structure and intensity of tropical cyclones using the high-resolution HWRF system. *J. Atmos. Sci*., **70**, 524–541, https://doi.org/10.1175/jas-d-11-0340.1.

Graham, K., 2019: Water impacts from recent U.S. landfalling tropical cyclones. National Hurricane Center, https://www.nhc.noaa.gov/outreach/presentations/FLGHC_2019_Keynote.pdf.

Gray, W. M., 1968: Global view of the origin of tropical disturbances and storms. *Mon. Wea. Rev.*, **96**, 669-700, https://doi.org/10.1175/1520-0493(1968)096%3C0669:GVOTOO%3E2.0.CO;2.

Gray, W. M., 1977: Tropical cyclone genesis in the western North Pacific. *J. Meteor. Soc. Japan*, **55**, 465-482, https://doi.org/10.2151/jmsj1965.55.5_465.

Gray, W. M., 1998: The formation of tropical cyclones. *Meteorl. Atmos. Phys.,* **67**, 37–69, https://doi.org/10.1007/BF01277501.

Hartmann, D. L., and E. D. Maloney, 2001: The Madden–Julian oscillation, barotropic dynamics, and North Pacific tropical cyclone formation. Part I: Observations. *J. Atmos. Sci.*, **58**, 2545–2558, https://doi.org/10.1175/1520-0469(2001)058<2545:TMJOBD>2.0.CO;2.

Halperin, D. J., H. E. Fuelberg, R. E. Hart, J. H. Cossuth, P. Sura, and R. J. Pasch, 2013: An evaluation of tropical cyclone genesis forecasts from global numerical models. *Wea. Forecasting*, **28**, 1423–1445, https://doi.org/10.1175/waf-d-13-00008.1.

Hazelton, A., et al., 2022: Performance of 2020 real-time atlantic hurricane forecasts from high-resolution global-nested hurricane models: HAFS-globalnest and GFDL T-SHiELD. *Wea. Forecasting*, **37**, 143–161, https://doi.org/10.1175/WAF-D-21-0102.1.

Hendricks, E. A., M. T. Montgomery, and C. A. Davis, 2004: The role of "vortical" hot towers in the formation of tropical cyclone Diana (1984). *J. Atmos. Sci*., **61**, 1209–1232, https://doi.org/10.1175/1520-0469(2004)061<1209:TROVHT>2.0.CO;2.

Ko, M.-C., F. D. Marks, G. J. Alaka Jr., and S. G. Gopalakrishnan, 2020: Evaluation of Hurricane Harvey (2017) rainfall in deterministic and probabilistic HWRF forecasts. *Atmos.*, **11**, 666, https://doi.org/10.3390/atmos11060666.

Latto, A., and R. Berg, 2022: Tropical storm Imelda. National Hurricane Center Tropical Cyclone Report. Accessed 12 October 2022, https://www.nhc.noaa.gov/data/tcr/.

Madden, R. A., and P. R. Julian, 1971: Detection of a 40–50 day oscillation in the zonal wind in the Tropical Pacific. *J. Atmos. Sci.*, **28**, 702–708, https://doi.org/10.1175/1520-0469(1971)028<0702:doadoi>2.0.co;2.

Madden, R. A., and P. R. Julian, 1972: Description of global-scale circulation cells in the tropics with a 40–50 day period. *J. Atmos. Sci.*, **29**, 1109–1123, https://doi.org/10.1175/1520-0469(1972)029<1109:dogscc>2.0.co;2.

Madden, R. A., and P. R. Julian, 1994: Observations of the 40–50-day tropical oscillation—A review. *Mon. Wea. Rev.*, **122**, 814–837, https://doi.org/10.1175/1520-0493(1994)122<0814:ootdto>2.0.co;2.

Marchok, T. P., 2002: How the NCEP tropical cyclone tracker works. *25th Conf. on Hurricanes and Tropical Meteorology*, San Diego, CA, Amer. Meteor. Soc., P1.13, https://ams.confex.com/ams/25HURR/webprogram/Paper37628.html.

Matsuno, T., 1966: Quasi-geostrophic motions in the equatorial area. *J. Meteor. Soc. Japan. Ser. II*, **44**, 25–43, https://doi.org/10.2151/jmsj1965.44.1_25.

McBride, J. L., and R. Zehr, 1981: Observational analysis of tropical cyclone formation. Part II: Comparison of non-developing versus developing systems. *J. Atmos. Sci.,* **38**, 1132–1151, https://doi.org/10.1175/1520-0469(1981)038<1132:oaotcf>2.0.co;2.

McTaggart-Cowan, R., T. J. Galarneau, L. F. Bosart, R. W. Moore, and O. Martius, 2013: A global climatology of baroclinically influenced tropical cyclogenesis. *Mon. Wea. Rev*., **141**, 1963–1989, https://doi.org/10.1175/MWR-D-12-00186.1.

Mehra, A., V. Tallapragada, Z. Zhang, B. Liu, L. Zhu, W. Wang, and H. Kim, 2018: Advancing the state of the art in operational tropical cyclone forecasting at NCEP. *Trop. Cyclone Res. Rev*., **7**, 51–56, https://doi.org/10.6057/2018TCRR01.06.

Mohazzabi, P., J. A. Smith Jones, and A. Citati, 2022: Thermodynamics of hurricanes revisited. *J. Appl. Math. Phys.*, **10**, 2508–2515, https://doi.org/10.4236/jamp.2022.108169.

Montgomery, M. T., M. E. Nicholls, T. A. Cram, and A. B. Saunders, 2006: A vortical hot tower route to tropical cyclogenesis. *J. Atmos. Sci.*, **63**, 355–386, https://doi.org/10.1175/jas3604.1.

National Weather Service, n.d.: Tropical cyclone structure. National Weather Service. Accessed 30 August 2019, https://www.weather.gov/jetstream/tc_structure.

National Weather Service, 2021: National hurricane center forecast verification. National Hurricane Center and Central Pacific Hurricane Center. Accessed 25 April 2022, https://www.nhc.noaa.gov/verification/.

NOAA National Centers for Environmental Information, 2022: U.S. billion-dollar weather and climate disasters. Accessed 12 October 2022, https://www.ncei.noaa.gov/access/billions.

NOAA National Hurricane Center, n.d.: Glossary of NHC terms, Accessed 12 October 2022, https://www.nhc.noaa.gov/aboutgloss.shtml.

Palmén, E., 1948: On the formation and structure of tropical hurricanes. *Geophysica*, **3**, 26-38.

Pasch, R. J., E. S. Blake, J. G. Jiing, M. M. Mainelli, and D. P. Roberts, 2008: Performance of the GFS in predicting tropical cyclone genesis during 2007. *28th Conf. on Hurricanes and Tropical Meteorology,* Orlando, FL, Amer. Meteor. Soc., 11A.7, https://ams.confex.com/ams/28Hurricanes/techprogram/paper_138218.htm.

Pasch, R. J., A. B. Penny, and R. Berg, 2019: Hurricane Maria. National Hurricane Center, https://www.nhc.noaa.gov/data/tcr/.

Peng, M. S., B. Fu, T. Li, and D. E. Stevens, 2012: Developing versus nondeveloping disturbances for tropical cyclone formation. Part I: North Atlantic. *Mon. Wea. Rev.*, **140**, 1047–1066, https://doi.org/10.1175/2011mwr3617.1.

Rappaport, E. N., and Coauthors, 2009: Advances and challenges at the National Hurricane Center. *Wea. Forecasting*, **24**, 395-419, https://doi.org/10.1175/2008WAF2222128.1.

Roberts, N., and H. Lean, 2008: Scale-selective verification of rainfall accumulations from high-resolution forecasts of convective events. *Mon. Wea. Rev.*, **136**, 78-97, https://doi.org/10.1175/2007MWR2123.1.

Rogers, R., F. Marks, and T. Marchok, 2009: Tropical cyclone rainfall. Encyclopedia of Hydrological Sciences. https://doi.org/10.1002/0470848944.hsa030.

Rogers, R., P. D. Reasor, J. A. Zawislak, and L. T. Nguyen, 2020: Precipitation processes and vortex alignment during the intensification of a weak tropical cyclone in moderate vertical shear. *Mon. Wea. Rev.,* **148**, 1899–1929, https://doi.org/10.1175/MWR-D-19-0315.1.

Seo, H., M. Jochum, R. Murtugudde, A. J. Miller, and J. O. Roads, 2008: Precipitation from African easterly waves in a coupled model of the tropical Atlantic. *J. Climate*, **21**, 1417–1431, https://doi.org/10.1175/2007JCLI1906.1.

Tallapragada, V., C. Kieu, Y. Kwon, S. Trahan, Q. Liu, Z. Zhang, and I.-H. Kwon, 2014: Evaluation of storm structure from the operational HWRF during 2012 implementation. *Mon. Wea. Rev*., **142**, 4308–4325, https://doi.org/10.1175/MWR-D-13-00010.1.

Tang, B. H., and Coauthors, 2020: Recent advances in research on tropical cyclogenesis. *Trop. Cyclone Res. Rev.*, **9**, 87–105, https://doi.org/10.1016/j.tcrr.2020.04.004.

Taylor, K. E., 2001: Summarizing multiple aspects of model performance in a single diagram. *J. Geophys. Res.*, **106**, 7183–7192, https://doi.org/10.1029/2000JD900719.

Ventrice, M. J., C. D. Thorncroft, and P. E. Roundy, 2011: The Madden–Julian oscillation's influence on African easterly waves and downstream tropical cyclogenesis. *Mon. Wea. Rev.*, **139**, 2704–2722, https://doi.org/10.1175/mwr-d-10-05028.1.

Ventrice, M. J., C. D. Thorncroft, and C. J. Schreck III, 2012: Impacts of convectively coupled Kelvin waves on environmental conditions for Atlantic tropical cyclogenesis. *Mon. Wea. Rev.*, **140**, 2198–2214, https://doi.org/10.1175/mwr-d-11-00305.1.

Walsh, K. J. E., M. Fiorino, C. W. Landsea, and K. L. McInnes, 2007: Objectively determined resolution-dependent threshold criteria for the detection of tropical cyclones in climate models and reanalyses. *J. Climate*, **20**, 2307–2314.

Wang, Z., 2012: Thermodynamic aspects of tropical cyclone formation. *J. Atmos. Sci*., **69**, 2433–2451, https://doi.org/10.1175/ JAS-D-11-0298.1.

Wang, Z., 2018: What Is the key feature of convection leading up to tropical cyclone formation? *J. Atmos. Sci.*, **75**, 1609–1629, https://doi.org/10.1175/jas-d-17-0131.1.

Wang, Z., and I. Hankes, 2016: Moisture and precipitation evolution during tropical cyclone formation as revealed by the SSM/I–SSMIS retrievals. *J. Atmos. Sci.*, **73**, 2773-2781, https://doi.org/10.1175/JAS-D-15-0306.1.

Wang, Z., A. Duan, S. Yang, and K. Ullah, 2017: Atmospheric moisture budget and its regulation on the variability of summer precipitation over the Tibetan Plateau. *J. Geophys. Res. Atmos.*, **122**, 614–630, https://doi.org/10.1002/2016JD025515.

Wang, Z., W. Li, M. S. Peng, X. Jiang, R. McTaggart-Cowan, and C. A. Davis, 2018: Predictive skill and predictability of North Atlantic tropical cyclogenesis in different synoptic flow regimes. *J. Atmos. Sci.,* **75**, 361–378, https://doi.org/10.1175/JAS-D-17-0094.1.

Wheeler, M., and G. N. Kiladis, 1999: Convectively coupled equatorial waves: Analysis of clouds and temperature in the wavenumber–frequency domain. *J. Atmos. Sci.*, **56**, 374–399, https://doi.org/10.1175/1520-0469(1999)056<0374:ccewao>2.0.co;2.

Wu, L., H. Su, R. G. Fovell, T. J. Dunkerton, Z. Wang, and B. H. Kahn, 2015: Impact of environmental moisture on tropical cyclone intensification. *Atmos. Chem. Phys.*, **15**, 14041–14053, https://doi.org/10.5194/acp-15-14041-2015.

Zawislak, J., 2020: Global survey of precipitation properties observed during tropical cyclogenesis and their differences compared to nondeveloping disturbances. *Mon. Wea. Rev.,* **148**, 1585–1606, https://doi.org/10.1175/mwr-d-18-0407.1.

Zhang, W., B. Fu, M. Peng, and T. Li, 2015: Discriminating developing versus nondeveloping tropical disturbances in the Western North Pacific through decision tree analysis. *Wea. Forecasting*, **30**, 446–454, https://doi.org/10.1175/WAF-D-14-00023.1.

Zhang, X., S. G. Gopalakrishnan, S. Trahan, T. S. Quirino, Q. Liu, Z. Zhang, G. J. Alaka, and V. Tallapragada, 2016: Representing multiple scales in the Hurricane Weather Research and Forecasting modeling system: Design of multiple sets of movable multilevel nesting and the basin-scale HWRF forecast application. *Wea. Forecasting*, **31**, 2019–2034, https://doi.org/10.1175/WAF-D-16-0087.1.